The timing of basaltic volcanism at the Apollo landing sites

Available online at www.sciencedirect.com

ScienceDirect

Geochimica et Cosmochimica Acta xxx (2019) xxx–xxx

Geochimica et Cosmochimica Acta

www.elsevier.com/locate/gca

The timing of basaltic volcanism at the Apollo landing sites

Joshua F. Snape [a,b,*], Alexander A. Nemchin [c], Martin J. Whitehouse [a], Renaud E. Merle [a], Thomas Hopkinson [d], Mahesh Anand [d,e]

[a] Department of Geosciences, Swedish Museum of Natural History, SE-104 05 Stockholm, Sweden
[b] Faculty of Earth and Life Sciences, VU Amsterdam, De Boelelaan 1085, 1081 HV Amsterdam, the Netherlands
[c] Department of Applied Geology, Curtin University, Perth, WA 6845, Australia
[d] School of Physical Science, The Open University, Milton Keynes MK7 6AA, United Kingdom
[e] Department of Earth Sciences, The Natural History Museum, London SW7 5BD, United Kingdom

Received 10 January 2019; accepted in revised form 23 July 2019; available online xxxx

Abstract

Precise crystallisation ages have been determined for a range of Apollo basalts from Pb-Pb isochrons generated using Secondary Ion Mass Spectrometry (SIMS) analyses of multiple accessory phases including K-feldspar, K-rich glass and phosphates. The samples analysed in this study include five Apollo 11 high-Ti basalts, one Apollo 14 high-Al basalt, seven Apollo 15 low-Ti basalts, and five Apollo 17 high-Ti basalts. Together with the samples analysed in two previous similar studies, Pb-Pb isochron ages have been determined for all of the major basaltic suites sampled during the Apollo missions. The accuracy of these ages has been assessed as part of a thorough review of existing age determinations for Apollo basalts, which reveals a good agreement with previous studies of the same samples, as well as with average ages that have been calculated for the emplacement of the different basaltic suites at the Apollo landing sites. Furthermore, the precision of the new age determinations helps to resolve distinctions between the ages of different basaltic suites in more detail than was previously possible. The proposed ages for the basaltic surface flows at the Apollo landing sites have been reviewed in light of these new sample ages. Finally, the data presented here have also been used to constrain the initial Pb isotopic compositions of the mare basalts, which indicate a significant degree of heterogeneity in the lunar mantle source regions, even among the basalts collected at individual landing sites.

Keywords: lunar volcanism; mare basalt; Apollo; Pb isotopes; chronology

1. INTRODUCTION

Samples of lunar basalt provide a direct record for the magmatic evolution of the Moon. Previous studies of the basalt samples collected during the Apollo and Luna missions have determined crystallisation ages ranging from approximately 4300–3100 Ma, with the vast majority comprising the mare basalts collected during the Apollo 11, 12, 15 and 17 missions, which have been dated to between 3800 and 3100 Ma (Nyquist and Shih, 1992; for a more recent summary of lunar basalt ages see also Joy and Arai, 2013). The ages determined for the Apollo and Luna basalts also have important implications beyond just the timing of mare volcanism on the Moon, as they have provided chronological information to determine the relationship between the age of a geologic unit on a planetary surface and the density of impact craters on that surface (e.g., Fassett, 2016 and references therein). In the case of the Moon, crater counting statistics indicate that the exposed

* Corresponding author at: Faculty of Earth and Life Sciences, VU Amsterdam, De Boelelaan 1085, 1081 HV Amsterdam, the Netherlands.
E-mail address: j.f.snape@vu.nl (J.F. Snape).

https://doi.org/10.1016/j.gca.2019.07.042
0016-7037/

mare basalt units were emplaced between 4000 and 1200 Ma, with a peak in basalt emplacement between approximately 3700 and 3300 Ma (Hiesinger et al., 2003, 2010).

Beyond defining the duration of volcanic activity on the Moon, these ages have also provided insights into the evolving chemical nature of lunar volcanism. For example, the oldest pristine basalt samples (i.e. excluding clasts identified in impact breccias) in the Apollo collection are the Apollo 14 high-Al basalts (~3950 Ma; Papanastassiou and Wasserburg, 1971a; Turner et al., 1971; Compston et al., 1972; Stettler et al., 1973), and the KREEP-rich (a geochemical signature defined by elevated concentrations of K, Rare Earth Elements, and P) basaltic samples from the Apollo 15 mission (~3900 Ma; Turner et al., 1973; Stettler et al., 1973; Nyquist et al., 1979; Carlson and Lugmair, 1979). The formation of these rocks appears to have been followed by a protracted period of high-Ti (defined as basalts containing >6 wt% bulk rock TiO_2; Neal and Taylor, 1992) mare volcanism, as sampled by the Apollo 11 (~3600–3850 Ma; Snyder et al., 1994 and references therein) and Apollo 17 missions (~3700–3800 Ma; Paces et al., 1991 and references therein). Finally, the youngest mare basalts sampled by the Apollo missions are the low-Ti (1–6 wt% bulk rock TiO_2; Neal and Taylor, 1992) basalts collected at the Apollo 15 (~3300–3350 Ma; e.g., Papanastassiou and Wasserburg, 1973; Husain, 1974; Snyder et al., 1997, 1998) and Apollo 12 (~3200 Ma; Snyder et al., 1994 and references therein) landing sites. While the ages in the literature make it possible to assemble this broad timescale for the emplacement of the mare basalts, they typically do not provide sufficient resolution to investigate the timing of individual basalt suites, as defined by the elemental and isotopic compositions.

The vast majority of ages for the lunar basalts were determined by the ^{40}Ar-^{39}Ar, Rb-Sr and Sm-Nd methods (e.g., Turner, 1970; Papanastassiou et al., 1970; Papanastassiou and Wasserburg, 1971a, 1971b; Tatsumoto et al., 1972a; Husain, 1974; Nyquist et al., 1977, 1979, 1981; Guggisberg et al., 1979). Although analyses of the U-Pb system in zircon and Ca-phosphate phases has been demonstrated to be of great value in providing insights into the formation of some of the earliest igneous rocks on the Moon (e.g., Nemchin et al., 2008, 2009, 2012, Grange et al., 2009, 2013), and constraining the impact history of the Moon with new ages for lunar breccias (e.g., Merle et al., 2014, 2017; Snape et al., 2016a; Thiessen et al., 2017, 2018), the U-Pb system has previously provided limited insights into the chronology of mare basalts. A number of early studies did provide Pb isotopic data for a range of lunar samples, including mare basalts (Tatsumoto et al., 1970, 1972b; Tera and Wasserburg, 1972, 1974; Nunes et al., 1974; Unruh and Tatsumoto, 1977; Chen et al., 1978; Tilton and Chen, 1979), but these efforts were complicated by the radiogenic nature of the samples and their low Pb content (Premo et al., 1999; Nemchin et al., 2011). By comparison with the solution approaches taken in these previous efforts, Secondary Ion Mass Spectrometry (SIMS) allows for the *in situ* targeting of specific mineral phases in a geologic sample. Several recent studies (Snape et al., 2016b, 2018a, 2018b) have utilised this potential to obtain Pb isotopic data from a range of phases in different lunar basalts, particularly focusing on accessory phases such as K-feldspar, K-rich glass and phosphates in interstitial late stage assemblages, where Pb and U are most concentrated. The results of these analyses have been used to determine new precise crystallisation ages (2σ errors typically within ± 15 Ma) and initial Pb isotopic compositions of the basalts (Snape et al., 2016b, 2018a, 2018b).

In this study, an additional 18 mare basalt samples have been analysed, including samples from the Apollo 11, 14, 15 and 17 landing sites. Together with the Pb isotopic compositions and crystallisation ages published in two previous studies (Snape et al., 2016b, 2018a), this amounts to a total of 29 Apollo basalts that have been analysed using this approach, representing samples from all of the major mare basalt suites. The following discussion will compare these new crystallisation ages with those previously obtained for the mare basalts, and assess the implications of this dataset for the timing of mare volcanism, as sampled by the Apollo missions.

2. SAMPLES AND METHODS

2.1. Sample descriptions

The Apollo 11 high-Ti basalts are divided into the high-K ($K_2O > 0.2$ wt%) Group A samples and low-K ($K_2O < 0.1$ wt%) Group B samples (e.g., Beaty and Albee, 1978; Snyder et al., 1994; Jerde et al., 1994). The Group A basalts are represented in this study by sample 10049. Petrographic descriptions of the sample were previously presented by Schmitt et al. (1970) and McGee et al. (1977), who referred to the sample as being a fine-grained (typically < 0.10 mm grainsize), vesicular to vuggy basalt comprising intergrown crystals of anhedral pyroxene (45–50% modal abundance; 0.02–0.08 mm), plagioclase (35–40%; 0.03–1.10 mm), ilmenite (15–20%; 0.01–0.10 mm) and rare olivine (0.1–0.3 mm). The section analysed in this study (10049, 121; Fig. A.1) is broadly consistent with this description, although the plagioclase grains were all smaller (~0.01–0.40 mm) than the larger grains previously reported. The low-K, Group B, Apollo 11 samples are sub divided based on additional textural, mineralogical, and compositional characteristics into the Group B1, B2 and B3 basalts (Beaty and Albee, 1978), which are all represented in this study. Additionally, several small basaltic soil fragments from Apollo 11 were identified as representing a separate anomalous category of low-K basalts (Group D; Beaty et al., 1979; Jerde et al., 1994; Snyder et al., 1996), which were not analysed in this study. Lead isotopic data, including a well-defined Pb-Pb isochron and initial Pb composition, was previously reported for the Group B1 basalt, 10044 (Snape et al., 2016b). In this study an additional Group B1 basalt, 10058, was analysed. The two sections of this sample analysed in this study (10058, 254 and 10058, 260; Fig. A.1) are consistent with the petrographic description given by Schmitt et al. (1970), as being a

Please cite this article in press as: Snape J. F., et al. The timing of basaltic volcanism at the Apollo landing sites. *Geochim. Cosmochim. Acta* (2019), https://doi.org/10.1016/j.gca.2019.07.042

medium grained (1.0–2.0 mm) ophitic basalt, formed of plagioclase (40%), pyroxene (35%), ilmenite (15%) and cristobalite (10%). The Group B2 basalts are represented in this study by a single sample, 10003. The medium-grained (~0.1–0.8 mm) section analysed here (10003, 199; Figs. 1 and A.1) is more consistent with the subophitic description given by Schmitt et al. (1970), than the porphyritic description given by McGee et al. (1977). Two Group B3 basalts (10020 and 10045) were analysed, both of which were previously described as fine-grained ophitic to porphyritic basalts (Schmitt et al., 1970; McGee et al., 1977; Beaty and Albee, 1978). The sections analysed here (10020, 258 and 10045, 199; Figs. A.1) are characterised by phenocrysts of pyroxene (~0.1–0.4 mm) and olivine (~0.3–1.5 mm), plus plagioclase and ilmenite that are present as either laths (typically 0.04 × 0.50 mm) or less elongated, tabular grains (0.1 × 0.2 mm), and small (0.01–0.04 mm) grains of a silica polymorph, which is most likely cristobalite, based on previous studies (e.g., Beaty and Albee, 1978).

In addition to the data presented previously for 14072 (Snape et al., 2016b), a second Apollo 14 high-Al basalt, 14053, has been analysed in this study. The section analysed here (14053, 299; Fig. 1 and A.1) resembles those analysed in previous studies, which described the sample as a coarse-grained (0.5–2.0 mm) ophitic basalt composed of clinopyroxene (50%), plagioclase (40%), ilmenite (2–4%), cristobalite (2–3%), olivine (2–4%) and minor amounts (<1%) of Fe-metal and mesostasis (e.g., Gancarz et al., 1971; Kushiro et al., 1972; Papike et al., 1976; Taylor et al., 2004).

Two main groups of basalts are identified in the Apollo 15 sample collection: (1) the olivine-normative basalts, which are represented in this study by samples 15016, 15555, 15557; and (2) the quartz-normative basalts (sometimes referred to as pigeonite basalts), represented here by samples 15058, 15065 and 15085. The olivine-normative basalt, 15016, is highly vesicular, as evidenced by the section analysed in this study (15016, 14; Fig. A.1), with phenocrysts of pyroxene (~0.5–1.5 mm) and olivine (~0.1–0.6 mm), as well as subophitic intergrowths of pyroxene and plagioclase, with the plagioclase being present both as laths (typically 1.0 × 0.2 mm) and smaller (~0.25 mm) more blocky crystals. Previous studies have determined the mineralogical mode for the sample as comprising pyroxene (64–67%), plagioclase (20–22%), olivine (7–8%), ilmenite (6%) and minor amounts (<1%) of silica, chromite, ulvöspinel and mesostasis (Papike et al., 1976; McGee et al., 1977). Samples 15555 and 15557 have been determined to have similar mineralogical modes of pyroxene (40–65%), plagioclase (25–35%), olivine (5–20%), opaques (including ilmenite, chromite and ulvöspinel; 3–5%), mesostasis (up to 5%) and cristobalite (up to 2%), based on several previous studies (Longhi et al., 1972; Brown et al., 1972; Nord et al., 1973; McGee et al., 1977). The section of sample 15555 anlaysed here (15555, 142; Fig. A.1) is composed of rounded to subhedral phenocrysts of olivine and pyroxene (both ~0.5–1.5 mm in size), embedded in poikilitic plagioclase (up to ~1.5 mm). Sample 15557 (represented here by section 15557, 154; Fig. A.1) is generally finer grained than 15555, with an intergranular texture of plagioclase and pyroxene (both between ~0.05 and 0.50 mm), olivine grains (~0.2–1.2 mm). The three quartz-normative basalts studied here (15058, 89; 15065, 90; 15085, 56; Figs. 1 and A.1) are all characterised by large (up to 2.0 cm) phenocrysts of pyroxene, surrounded by coarse-grained (~0.1–1.0 mm) subophitic intergrowth of pyroxene and plagioclase. The mineralogical mode of these three samples were determined in several previous studies (Butler, 1971; Longhi et al., 1972; Brown et al., 1972; Papike et al., 1976) as pyroxene (40–71%), plagioclase (24–60%), opaques (1–4%) and silica (1–3%). In addition to the two main groups of low-Ti basalts collected by Apollo 15, there are several small and compositionally distinct samples described as picritic basalts. The picritic basalt analysed in this study, 15385 (section 15385, 9; Fig. A.1) has a similar intergranular texture to the olivine-normative basalt, 15557, with subhedral olivine and pyroxene phenocrysts (ranging in size from ~0.1 to 1.5 mm and with a modal abundance of 30% and 42%, respectively; Dowty et al., 1973), embedded in plagioclase (24%; Dowty et al., 1973).

The Apollo 17 high-Ti mare basalts are divided into three main compositional groups (Groups A, B and C; Rhodes et al., 1976; Warner et al., 1979; Paces et al., 1991). An additional subdivision of the Type B basalts has previously been proposed (Neal et al., 1990), and an anomalous sample (79001, 2144) was suggested to be part of a separate basaltic group (Group D; Ryder 1990). For the purposes of this study, the samples were selected to focus on the three main groups, with two Group A basalts (75035 and 75055), two Group B basalts (70017 and 75075), and one Group C basalt (74275). The analysed sections of the Group A basalts (75035, 210, 75055, 57 and 75055, 8; Figs. 1 and A.1) are typical of those described previously, and are primarily composed of pyroxene (45–50%; Brown et al., 1975), subophitically enclosing crystals of plagioclase and ilmenite, which commonly form laths (up to 2.5 mm in length) as well as some less elongated anhedral grains (~0.1–1.0 mm). The two Group B basalt sections (70017, 42 and 75075, 9; Fig. A.1) have similar textures with relatively large (~0.05–0.50 mm) grains of ilmenite with embayed edges, that are completely or partially enclosed within subhedral grains of pyroxene (~0.1–1.0 mm), and occasional grains of olivine (~0.3–0.5 mm), all of which are poikilitically surrounded by plagioclase (up to ~2.0 mm). Brown et al. (1975) reported similar mineralogical modes for both samples: pyroxene (49–52%), plagioclase (21–25%), opaques (primarily ilmenite; 23–24%), cristobalite (1–2%) and minor mounts (<1%) of mesostasis. Finally, the section of the Group C basalt analysed here (74275, 357; Fig. A.1), contains phenocrysts of olivine and pyroxene (~0.1–1.0 mm), in addition to composite grains of armalcolite with ilmenite mantles and embayed edges forming either small (<0.2 mm) equant crystals or laths (up to 1.0 mm), and euhedral chromite crystals (<0.1 mm) occasionally forming glomerophyric clusters, all within a fine-grained (<0.1 mm) subophitic and occasionally variolitic groundmass of plagioclase, pyroxene and interstitial silica and mesostasis. Brown et al. (1975) reported a mineralogical mode for 74275 of pyroxene (36%), opaques (31%), plagioclase (19%) and olivine (13%).

Please cite this article in press as: Snape J. F., et al. The timing of basaltic volcanism at the Apollo landing sites. *Geochim. Cosmochim. Acta* (2019), https://doi.org/10.1016/j.gca.2019.07.042

2.2. Analytical protocol

The majority of the sections analysed were prepared as rock chips in polished epoxy mounts, although exceptions to this were the thin sections 10058, 254, 75055, 8, 15016, 14, 15385, 9 and 15065, 90. All of the analysed samples were prepared at NASA Johnson Space Center. Each sample was cleaned with ethanol before being carbon coated. Backscattered electron (BSE) images and elemental maps of each section (Fig. A.1) were acquired using a Quanta 650 FEGSEM and accompanying Oxford Instruments Energy Dispersive Spectroscopy (EDS) detector at Stockholm University, operating with an accelerating voltage of 20 kV at a working distance of 10 mm. These images were used to identify suitable target areas for the SIMS analyses (examples of these are shown in Fig. 1). A priority in this target selection was to identify phases that would contain initial Pb (e.g., K-feldspar), as well as those containing radiogenic Pb generated from *in situ* decay of U since crystallisation of the sample (e.g., Ca-phosphates and Zr-rich phases). This variation helps to populate the different ends of the sample isochron, resulting in a more precise age determination. The target areas within these phases were selected to be large enough to accommodate a SIMS analytical spot (in this case the smallest spot used was ~10 μm), while avoiding any obvious cracks or voids in the sample, which would be likely places for terrestrial contamination to accumulate during sample polishing and cleaning procedures. Despite these efforts it was difficult to ensure that the SIMS spots did not overlap with small cracks not visible in the SEM images, or did not depth-profile into such features lying just below the original surface of the sample. Furthermore, given the low Pb concentrations in many of the analysed phases (particularly those with less radiogenic Pb isotope compositions), these analyses are particularly susceptible to even low levels of terrestrial contamination.

Following the SEM documentation of the samples and prior to the SIMS analyses, the samples were cleaned with a fine (1 μm) diamond paste and ethanol to remove the carbon coating before adding a 30 nm gold coating. The Pb isotopic compositions (complete dataset presented in Table B.1) of the phases were determined over six analytical sessions using a CAMECA IMS 1280 ion microprobe at the NordSIMS facility, Swedish Museum of Natural History, Stockholm, using a methodology similar to that outlined in previous studies (Whitehouse et al., 2005; Bellucci et al., 2015). Apertures in the primary column were used to generate a slightly elliptical O_2^- sample probe with dimensions appropriate to the target. The smaller accessory phases (including K-feldspar and phosphates) were analysed using a ~10 μm spot (beam current 2–5 nA), whereas larger grains (including plagioclase and K-rich glass) were analysed with a ~30 μm spot (beam current 14–16 nA). Prior to each measurement, an area of 20–35 μm around the spot location was rastered for at least 120 s in order to remove the gold coating and minimise possible surface contamination. The instrument was operated in high-transmission mode, corresponding to a transfer magnification of 160×. In this mode, the field aperture size was chosen to limit the field of view on the sample surface (i.e. the area from which ions will be admitted to the mass spectrometer) to be slightly larger than the spot but smaller than the rastered area, further minimising the possibility of measuring surface contamination. The mass spectrometer was operated with a nominal mass resolution of 4860 ($M/\Delta M$), sufficient to resolve Pb from known molecular interferences. A nuclear magnetic resonance (NMR) field sensor regulated the stability of the magnetic field to high precision. The Pb isotopes were measured simultaneously in multi-collector mode using four low-noise (<0.006 counts per second) ion counting electron multipliers (Hamamatsu 416) with electronically-gated deadtimes of 65 ns. Individual analyses were filtered out of the final dataset if the count rate for ^{206}Pb was less than one count per second. Background counts for each channel were measured at regular intervals during each session by using deflector and aperture settings that effectively blank both primary and any residual secondary beams. The average background values are reported in Table B.2.

Analyses of the USGS basaltic glass reference material, BCR-2G, were used to generate a correction factor to account for mass fractionation and detector relative gain calibration in the unknown analyses, using the values of Woodhead and Hergt (2000). This correction procedure involved dividing each of the "accepted" isotope ratios for BCR2-G (determined independently using TIMS analyses; Woodhead and Hergt, 2000), by the corresponding average of each ratio obtained from all standards in a given session in order to obtain a ratio-specific correction factor that incorporates both mass bias (a few parts per thousand at Pb mass; Shimizu and Hart, 1982) and inter-detector (a few percent) gain (Table B.3.). Isotope ratios of unknown samples were then corrected by multiplying by these factors. Within uncertainty limits, no systematic drift was observed in the BCR2-G measurements during a given analytical session, with the 1σ standard deviations from the average session values all being less than 1% (the complete set of average session values and associated standard deviations are reported in Table B.3).

The uncertainties stated for each ratio in the individual sample measurements (Table B.1) are derived from the internal run error propagated together with the standard deviations of the BCR-2G analyses for the relevant analytical session and the uncertainty given for the published BCR-2G values (Woodhead and Hergt, 2000). The errors stated for the Pb-Pb isochron dates in the following results and discussion sections are quoted at the 95% confidence level.

2.3. Data processing

The data were processed using in-house SIMS data reduction spreadsheets and the Excel add-in Isoplot (version 4.15; Ludwig, 2008), using the same approach as that outlined in Snape et al. (2016b). Briefly, the Pb isotopic compositions measured in each sample (Table B.1.) are interpreted as representing a mixture between three main components: (1) initial Pb present in the basaltic melt when it crystallised, (2) radiogenic Pb formed by the decay of U in the basalt after crystallisation, and (3) terrestrial contam-

Please cite this article in press as: Snape J. F., et al. The timing of basaltic volcanism at the Apollo landing sites. *Geochim. Cosmochim. Acta* (2019), https://doi.org/10.1016/j.gca.2019.07.042

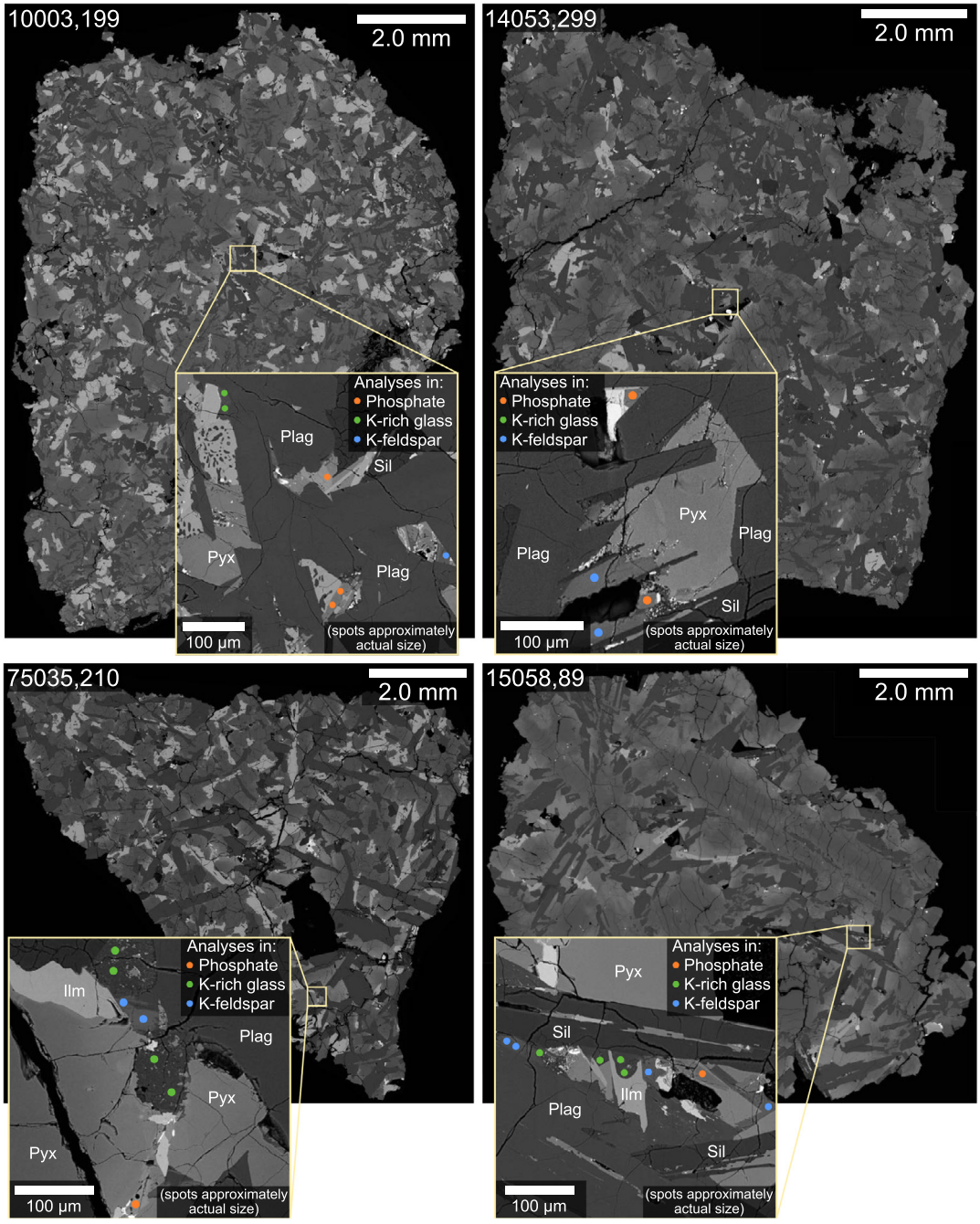

Fig. 1. Backscattered Electron (BSE) images illustrating four of the samples analysed and the typical areas targeted for the SIMS analyses. Plag – plagioclase; Pyx – pyroxene; Sil – silica; Ilm – ilmenite. (For interpretation of the colours in the figure(s), the reader is referred to the web version of this article.)

ination. These endmember components define a triangular array of points on a plot of $^{207}Pb/^{206}Pb$ vs. $^{204}Pb/^{206}Pb$ (two examples of this are shown in Fig. 2). The values with the highest $^{207}Pb/^{206}Pb$ ratios, at the top of the triangular array, will provide an estimate of the lowest possible value for the initial Pb composition of the sample. The radiogenic Pb component will be located where $^{204}Pb/^{206}Pb = 0$. Finally, given the radiogenic Pb isotopic compositions associated with the Moon relative to those found on Earth, the terrestrial contamination end-member will have the highest $^{204}Pb/^{206}Pb$ ratios. Based on this assumption, the bounding edge on the left side of the triangle, between the initial and radiogenic lunar Pb compositions, forms an isochron, which can be determined by iteratively filtering the data to yield the steepest statistically significant weighted regression (i.e. MSWD < 2; probability of fit, $P > 0.1$). Given that

Please cite this article in press as: Snape J. F., et al. The timing of basaltic volcanism at the Apollo landing sites. *Geochim. Cosmochim. Acta* (2019), https://doi.org/10.1016/j.gca.2019.07.042

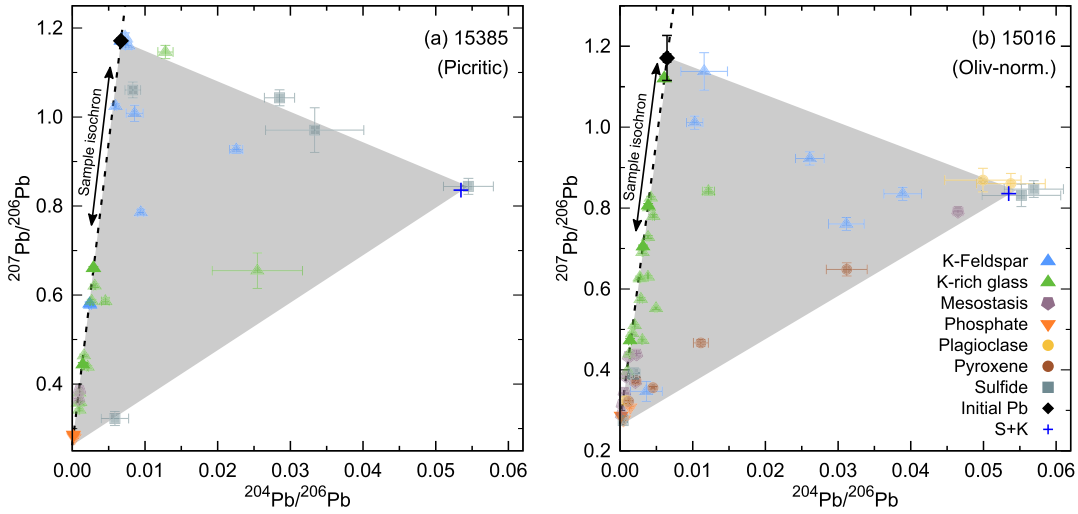

Fig. 2. $^{207}Pb/^{206}Pb$ vs. $^{204}Pb/^{206}Pb$ plots of the complete datasets from two Apollo 15 low-Ti basalts (a) 15385 and (b) 15016. The grey triangles represent the predicted range of compositions that would result from three-component mixing between the initial Pb isotopic compositions of the rocks, the more radiogenic Pb generated by the decay of U after the rocks formed, and a terrestrial contaminant (represented here with the model composition of modern terrestrial Pb presented by Stacey and Kramers (1975); "S + K"). Analyses (plotted in partially transparent symbols) lying to the right of sample isochron (i.e. the left side of the triangle) and within this mixing triangle are filtered out as containing significant amounts of terrestrial contamination.

the samples in this study are all pristine crystalline basalts, the dates defined by these isochrons are interpreted as representing the time of basalt crystallisation.

3. RESULTS

In general, the Ca-phosphates analysed throughout all of the samples (where present) have the most radiogenic compositions (i.e. with the lowest $^{207}Pb/^{206}Pb$ and $^{204}Pb/^{206}Pb$ ratios), indicating that a majority of the Pb in these phases is the result of *in situ* U decay since the basalt crystallised. By contrast, the K-feldspar and plagioclase analyses tend to yield less radiogenic compositions, with higher $^{207}Pb/^{206}Pb$ and $^{204}Pb/^{206}Pb$ ratios, indicating a higher proportion of initial Pb in these phases. This corresponds with studies of partitioning behaviour, where U is more compatible than Pb in phosphates (Prowatke and Klemme, 2006), whereas the opposite is true of K-feldspar and plagioclase (Blundy and Wood, 2003 and references therein). Analyses of the K-rich glass typically result in a range of Pb isotopic compositions, reflecting a mixture of the radiogenic and initial Pb endmember components. In a number samples (e.g. 10003, 10020, 14053, 15085; Fig. 3), K-feldspar grains appear to have quite radiogenic compositions, in some cases even more so than the K-rich glass. This is most likely the result of the SIMS spots unavoidably sampling other phases in these very fine-grained interstitial assemblages of late stage material, resulting in a mixed Pb isotopic composition.

The 18 Apollo basalts analysed in this study have a range of crystallisation ages from ~3250 to 3960 Ma, which are summarised in Table 1 and Figs. 3 and 4. The Apollo 11 high-Ti basalts have crystallisation ages of between ~3500 Ma and 3860 Ma. The youngest of these is the Group A basalt 10049 (Fig. 3a), with an age of 3578 ± 9 Ma (MSWD = 0.82; $P = 0.67$). The Group B1 basalt, 10058, has an age of 3697 ± 7 Ma (MSWD = 0.98; $P = 0.48$). The two Group B3 basalts analysed yielded similar ages of 3752 ± 18 Ma (sample 10020; MSWD = 0.52; $P = 0.79$) and 3747 ± 3 Ma (sample 10045; MSWD = 0.95; 0.54). The oldest crystallisation age determined for any of the Apollo 11 high-Ti basalts was from the Group B2 sample, 10003 (Fig. 3c), at 3854 ± 5 Ma (MSWD = 0.97; $P = 0.48$).

The oldest age (3955 ± 8 Ma; MSWD = 0.88; $P = 0.51$) was determined for the Apollo 14 high-Al basalt, 14053 (Fig. 3f). The youngest ages, meanwhile, come from the Apollo 15 low-Ti basalt samples, with the youngest of these being the picritic basalt, 15385 (Fig. 3m), with a crystallisation age of 3262 ± 14 Ma (MSWD = 0.99; $P = 0.41$). The three olivine normative basalts have ages of 3265 ± 16 Ma (sample 15555; MSWD = 1.4; $P = 0.21$), 3289 ± 9 Ma (sample 15016; MSWD = 0.47; $P = 0.80$) and 3290 ± 12 Ma (sample 15557; MSWD = 1.3; $P = 0.25$). The oldest Apollo 15 low-Ti mare basalts are the quartz normative samples, with ages of approximately 3360 Ma. Well-defined isochrons were obtained for two of these samples, indicating crystallisation ages of 3353 ± 6 Ma (sample 15085; MSWD = 0.55; $P = 0.96$), 3358 ± 9 Ma (sample 15058; MSWD = 0.68; $P = 0.77$). A third quartz normative sample, 15065, showed more significant signs of terrestrial contamination, with only three points that could be used to define an regression equating to an age of 3366 ± 44 Ma, and with a relatively poor statistical fit (MSWD = 2.6; $P = 0.11$). The most significant signs of terrestrial contamination in any of the samples analysed in this study are in three of the Apollo 15 basalts (15016, 15065 and 15385). Notably, the analysed sections of these samples were three

Please cite this article in press as: Snape J. F., et al. The timing of basaltic volcanism at the Apollo landing sites. *Geochim. Cosmochim. Acta* (2019), https://doi.org/10.1016/j.gca.2019.07.042

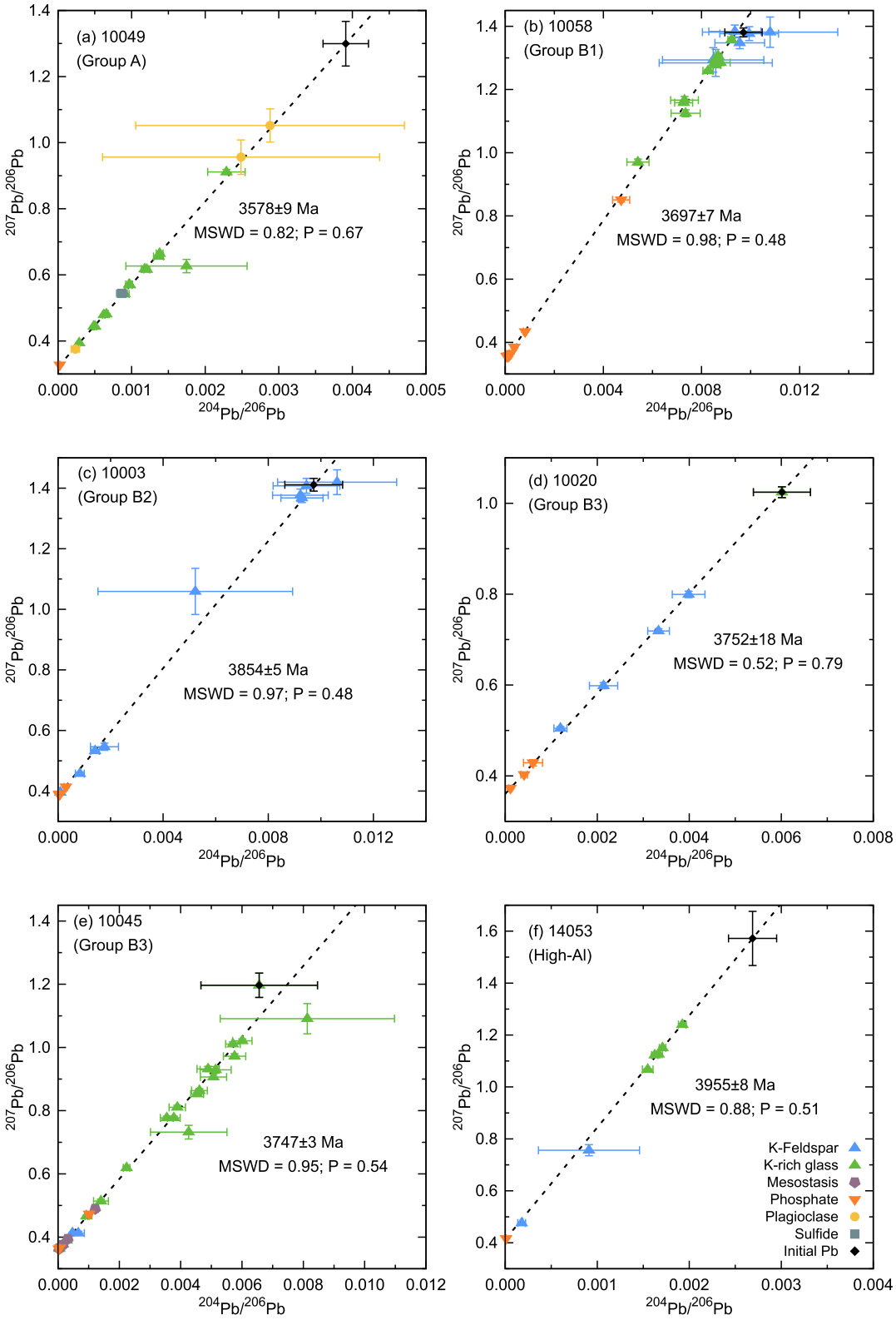

Fig. 3. $^{207}Pb/^{206}Pb$ vs. $^{204}Pb/^{206}Pb$ plots of the filtered data sets for the Apollo 11 (a–e), 14 (f), 15 (g–m) and 17 (n–r) basalts analysed. In the case of the Apollo 17 high-Ti basalt, 75055, an expanded subpanel illustrates how the inclusion of tranquillityite data obtained previously (Tartèse et al., 2013) helps anchor the radiogenic end of the isochron, resulting in the overall age of 3752 ± 9 Ma. Error bars represent 2σ uncertainties and uncertainties for the isochron dates are stated at the 95% confidence level.

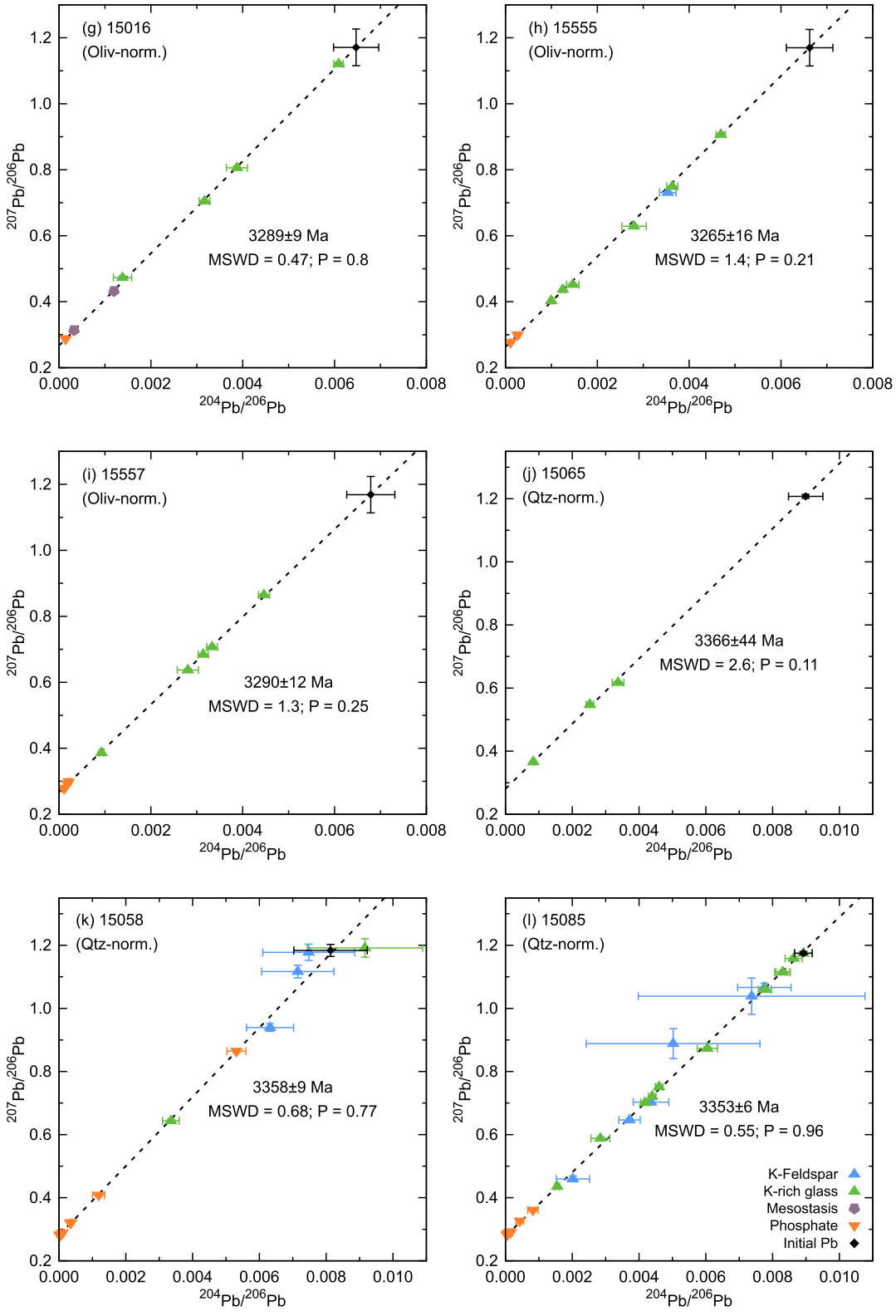

Fig 3. *(continued)*

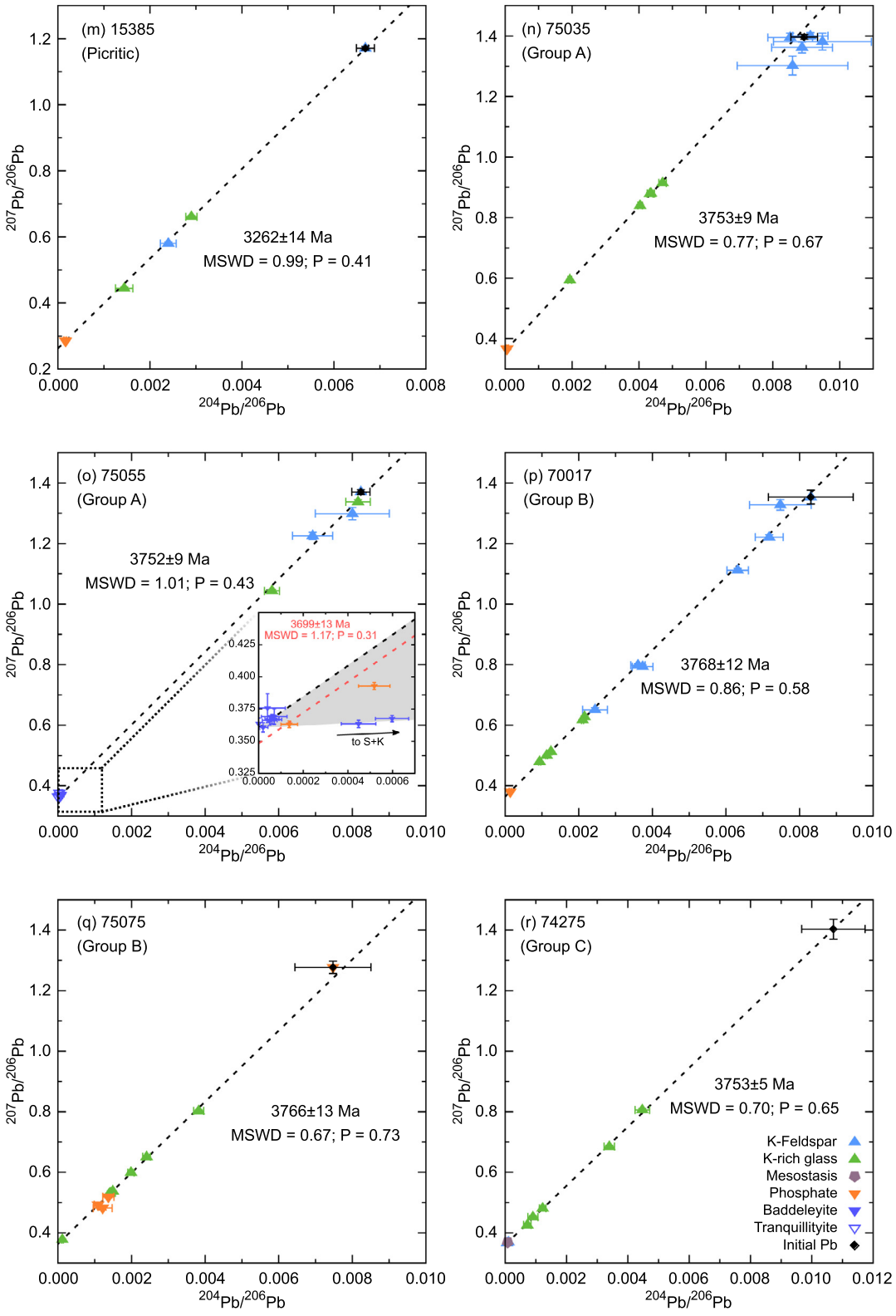

Fig 3. *(continued)*

Table 1
Summary of the crystallisation ages and initial Pb isotopic compositions for the Apollo basalts analysed in this study. The values for the samples published in previous studies are included for completeness, and are formatted in *italics* (Snape et al., 2016b, 2018a).

Sample		Basalt type	Age (Ma)	± (95% conf.)	Isochron details		Best estimates of initial composition*						
					MSWD	Prob.	No. of points	$^{204}Pb/^{206}Pb$	2σ	$^{207}Pb/^{206}Pb$	2σ	$^{208}Pb/^{206}Pb$	2σ
10049	§§	High-Ti, Group A	3578	9	0.82	0.67	19	0.0039	0.0003	1.299	0.068	(not determined)	
10044		*High-Ti, Group B1*	*3688*	*5*	*1.2*	*0.16*	*35*	*0.0099*	*0.0011*	*1.399*	*0.020*	*0.986*	*0.029*
10058		High-Ti, Group B1	3697	7	0.98	0.48	25	0.0097	0.0008	1.381	0.014	0.975	0.011
10003		High-Ti, Group B2	3854	5	0.97	0.48	14	0.0097	0.0011	1.411	0.021	1.002	0.016
10020	§	High-Ti, Group B3	3752	18	0.52	0.79	8	0.0060	0.0006	1.024	0.012	0.890	0.011
10045	§	High-Ti, Group B3	3747	3	0.95	0.54	31	0.0066	0.0019	1.197	0.039	(not determined)	
12002	§	*Low-Ti, Olivine*	*3167*	*12*	*1.3*	*0.23*	*12*	*0.0036*	*0.0001*	*1.083*	*0.006*	*0.851*	*0.005*
12012	§	*Low-Ti, Olivine*	*3151*	*21*	*1.4*	*0.13*	*17*	*0.0035*	*0.0002*	*1.064*	*0.007*	*0.894*	*0.006*
12039		*Low-Ti, Pigeonite*	*3129*	*10*	*0.65*	*0.89*	*23*	*0.0040*	*0.0002*	*1.152*	*0.005*	*0.890*	*0.004*
12021		*Low-Ti, Pigeonite*	*3176*	*6*	*1.2*	*0.26*	*16*	*0.0041*	*0.0002*	*1.106*	*0.007*	*0.97*	*0.33*
12005		*Low-Ti, Ilmenite*	*3182*	*10*	*1.5*	*0.15*	*11*	*0.0054*	*0.0003*	*1.190*	*0.008*	*0.933*	*0.038*
12016	§	*Low-Ti, Ilmenite*	*3188*	*11*	*1.19*	*0.26*	*19*	*0.0055*	*0.0005*	*1.171*	*0.011*	*0.909*	*0.009*
12063	§	*Low-Ti, Ilmenite*	*3193*	*11*	*1.4*	*0.12*	*20*	*0.0061*	*0.0005*	*1.146*	*0.010*	*0.915*	*0.009*
12038	§	*Low-Ti, Feldspathic*	*3242*	*13*	*1.4*	*0.11*	*22*	*0.0051*	*0.0005*	*1.166*	*0.011*	*1.014*	*0.010*
14053	§§	High-Al	3955	8	0.88	0.51	8	0.0027	0.0003	1.57	0.10	(not determined)	
14072		*High-Al*	*3904*	*7*	*1.09*	*0.37*	*14*	*0.0026*	*0.0004*	*1.464*	*0.015*	*0.900*	*0.230*
15386	§§	*KREEP*	*3884*	*77*	*5.3*	*0*	*8*	*0.0018*	*0.0002*	*1.448*	*0.021*	*(not determined)*	
15385		Low-Ti, Picritic	3262	14	0.99	0.41	6	0.0067	0.0002	1.171	0.006	0.938	0.005
15016	§	Low-Ti, Olivine normative	3289	9	0.47	0.8	7	0.0065	0.0005	1.171	0.056	(not determined)	
15555	§§	Low-Ti, Olivine normative	3265	16	1.4	0.21	9	0.0066	0.0005	1.170	0.055	(not determined)	
15557	§§	Low-Ti, Olivine normative	3290	12	1.3	0.25	8	0.0068	0.0005	1.169	0.055	(not determined)	
15065	§§	Low-Ti, Quartz normative/ pigeonite	3366	44	2.6	0.11	3	0.0090	0.0005	1.208	0.006	(not determined)	
15058		Low-Ti, Quartz normative/ pigeonite	3358	9	0.68	0.77	14	0.0081	0.0011	1.184	0.019	1.031	0.017
15085		Low-Ti, Quartz normative/ pigeonite	3353	6	0.55	0.96	24	0.0089	0.0003	1.175	0.005	1.437	0.007
75035		High-Ti, Group A	3753	9	0.77	0.67	13	0.0089	0.0004	1.397	0.008	0.978	0.006
75055		High-Ti, Group A	3752	9	1.01	0.43	12	0.0082	0.0002	1.371	0.008	(not determined)	
70017		High-Ti, Group B	3768	12	0.86	0.58	13	0.0083	0.0012	1.354	0.023	1.057	0.019
75075	§	High-Ti, Group B	3766	13	0.67	0.73	11	0.0075	0.0010	1.277	0.021	1.242	0.020
74275	§§	High-Ti, Group C	3753	5	0.7	0.65	8	0.0105	0.0009	1.379	0.008	(not determined)	

Values in italics were reported previously (Snape et al., 2016b, 2018a) and are included here for completeness.
§ Initial Pb estimate based on just one or two measurements.
§§ Best estimate of Initial Pb taken from the intercept of "initial-contaminant mixing line" with isochron.

Please cite this article in press as: Snape J. F., et al. The timing of basaltic volcanism at the Apollo landing sites. *Geochim. Cosmochim. Acta* (2019), https://doi.org/10.1016/j.gca.2019.07.042

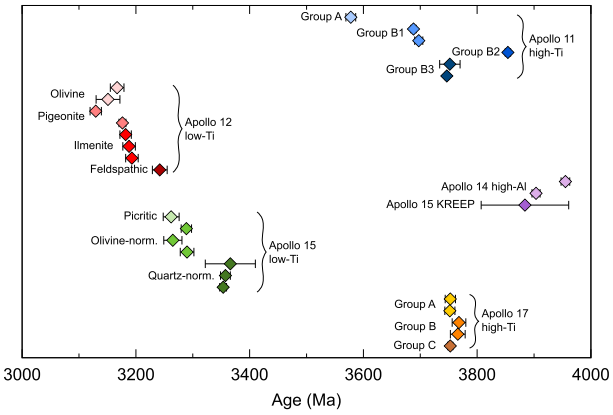

Fig. 4. Summary of all the Pb-Pb isochron ages determined the Apollo basalts analysed in this and two previous studies (Snape et al., 2016b, 2018b). Error bars are scaled to represent the 95% confidence level.

of only five older thin-sections used in the study (the other two thin sections being 10058, 254 and 75055, 8). The majority of the samples analysed were new polished epoxy mounts prepared at NASA JSC and analysed for the first time in this study. As such, it seems likely that these three Apollo 15 basalts are reflecting the accumulation of contamination from handling in different laboratories over the years.

The Apollo 17 Group A high-Ti basalt, 75035, has a crystallisation age of 3753 ± 9 Ma (MSWD = 0.77; $P = 0.67$). Based on the data in this study alone, the second Group A basalt sample, 75055, appears to have a younger crystallisation age of 3697 ± 13 Ma (MSWD = 0.81; $P = 0.54$). However, comparison with NanoSIMS analyses by Tartèse et al. (2013) of tranquillityite Pb isotopic compositions in one of the same thin sections that was used in this study (75055, 8), indicates that the most radiogenic analyses in this new dataset are slightly contaminated with terrestrial Pb and lie within the mixing triangle described in Section 2.3 (Fig. 3o). The Tartèse et al. (2013) study did not include analyses of phases with less radiogenic Pb isotopic compositions, and so could not accurately estimate the effects of a lunar initial Pb component, and the tranquillityite data from this study were originally used to calculate a $^{207}Pb/^{206}$-Pb age of 3772 ± 9 Ma, assuming any such effects to be negligible and within the uncertainties of the measurements. Combining those data with the results presented here resolves this uncertainty regarding the initial Pb component, and results in a crystallisation age of 3752 ± 9 Ma (MSWD = 0.82; $P = 0.60$) for 75055; identical to that of the 75035. Similar ages are also determined for the Group B basalts, 75075 (3766 ± 13 Ma; MSWD = 0.67; $P = 0.73$) and 70017 (3768 ± 12 Ma; MSWD = 0.86; $P = 0.58$), and the Group C basalt, 74275 (3753 ± 5 Ma; MSWD = 0.7; $P = 0.65$).

For many of the samples (10 out of 18), it was possible to obtain an estimate for the initial Pb composition (i.e. the lowest possible $^{204}Pb/^{206}Pb$ and $^{207}Pb/^{206}Pb$ ratios for the initial Pb components) directly from the least radiogenic analyses on the sample isochrons (i.e. the analyses resulting in the highest $^{204}Pb/^{206}Pb$ and $^{207}Pb/^{206}Pb$ ratios; Fig. 3). In several cases, it was clear that these least radiogenic analyses fell far short of the likely initial Pb composition, and an alternative approach was taken, by using several of the terrestrial Pb-contaminated data points in an attempt to define the mixing line between the composition of the terrestrial contaminant and the initial Pb component (Fig. 2; see also Table B.1. for details of the analyses used to calculate these mixing lines). For three of the analysed samples (15555, 15557 and 74275), there were not enough data points to define this mixing line, and so the estimations of the initial Pb isotopic compositions are based on the mixing lines defined from other similar samples (15016 for the two Apollo 15 samples, and 75055 in the case of 74275), making these estimations even less confident. A summary of the best estimates for the initial Pb isotopic compositions is provided in Table 1. More detailed information regarding these initial Pb isotopic compositions is provided in Table B.4, including both the estimates taken directly from sample measurements, and those determined by calculating the intercept of the initial-contamination mixing line and the sample isochron.

Plots of the $^{208}Pb/^{206}Pb$ ratios against $^{204}Pb/^{206}Pb$ and $^{207}Pb/^{206}Pb$ for the filtered datasets from each of the samples lie on a plane in the 3D coordinate space, with the initial Pb compositions converging at similar $^{208}Pb/^{206}Pb$ ratios (0.89–1.07) for samples from all of the different basaltic suites and landing sites (Fig. 5). The measurements of phases containing more Pb from *in situ* radiogenic decay spread out, with the most radiogenic endmember compositions between $^{208}Pb/^{206}Pb \sim 0.2$–3.1 (Fig. 5). This range in radiogenic $^{208}Pb/^{206}Pb$ ratios is interpreted as variability in $^{232}Th/^{238}U$ ratios between different mineral phases within the samples. Taking the different crystallisation ages of the samples into account, these $^{208}Pb/^{206}Pb$ values would correspond to $^{232}Th/^{238}U$ ratios of between ~0 and 3.0.

4. DISCUSSION

4.1. Comparison with previous Pb isotopic analyses

Comparison of the data presented here with previous Pb isotopic analyses of the same basalt samples (Tatsumoto et al., 1970, 1972b; Tera and Wasserburg, 1972, 1974; Nunes et al., 1974; Unruh and Tatsumoto, 1977; Chen et al., 1978; Tilton and Chen, 1979) is consistent with the three-component mixing assumption (Section 2.3), which forms the basis for the definition of the Pb-Pb isochrons. For each case, the Pb isotopic compositions determined previously lie either on or to the right of the sample isochron, within the mixing triangle defined by the three components (Fig. 6). It should be noted that lunar rocks have generally low Pb abundances and that these previous data were typically obtained as whole rock compositions, or from separates of major silicate phases and ilmenite, while the vast majority of SIMS data used to generate the isochrons in this study was obtained from accessory phases. Therefore, this observation of previously determined Pb isotopic compositions containing varying amounts of ter-

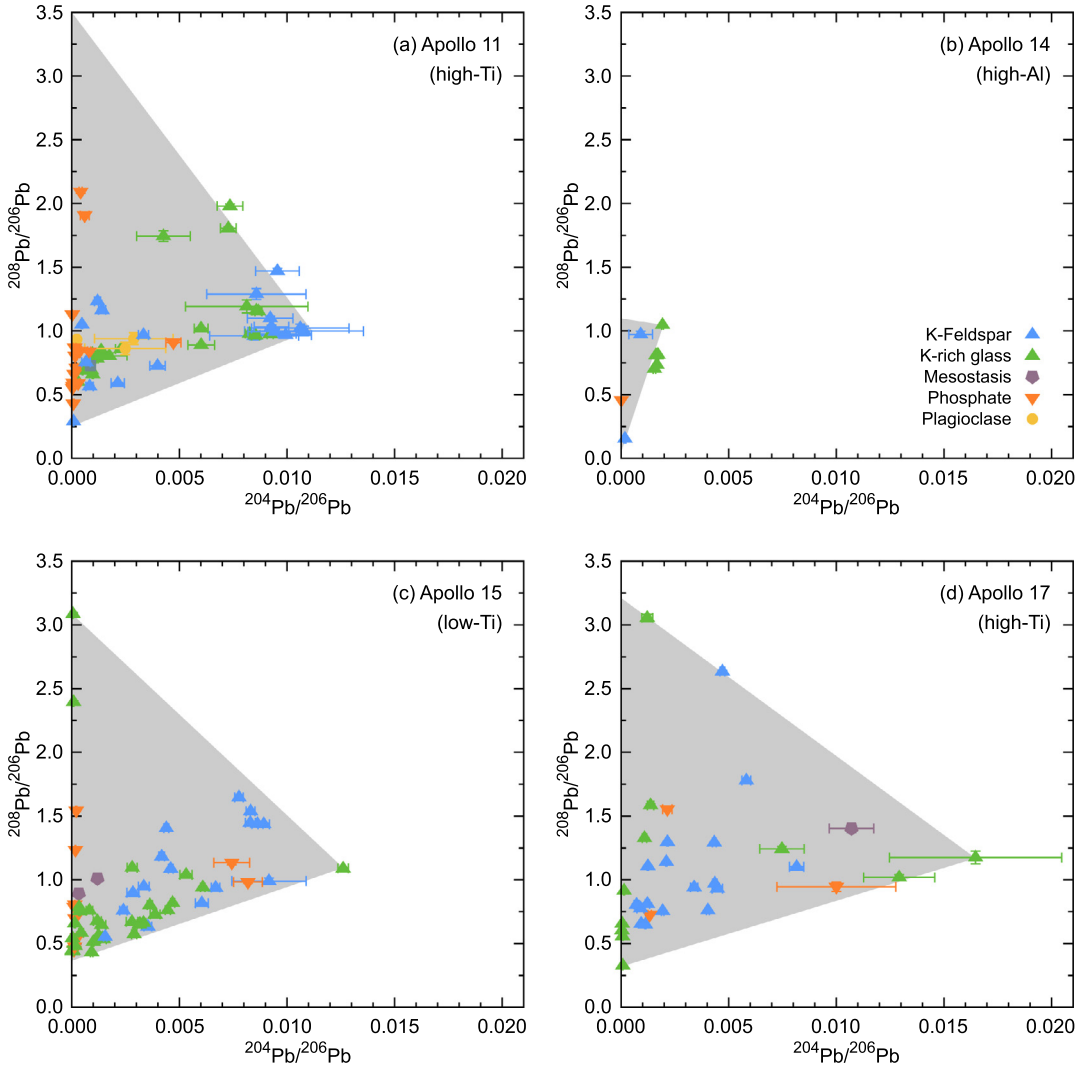

Fig. 5. $^{208}Pb/^{206}Pb$ vs. $^{204}Pb/^{206}Pb$ plots of the filtered data sets for the Apollo 11 (a), Apollo 14 (b), Apollo 15 (c) and Apollo 17 (c) basalts. Grey triangular fields mark the range of compositions in each group of samples. The least radiogenic compositions converge at similar $^{208}Pb/^{206}Pb$ ratios of 0.89–1.07. Taking into account the ages of the individual samples, the range of $^{208}Pb/^{206}Pb$ ratios in the most radiogenic compositions (~0.2–3.1) correspond to $^{232}Th/^{238}U$ ratios of between ~0 and 3.0. Error bars represent 2σ uncertainties.

restrial Pb contamination is not surprising and reflects the ability of the *in situ* analytical approach taken here to sample phases that could not be analysed in isolation in previous studies.

4.2. Comparison with previous age determinations

In order to compare the crystallisation ages determined by the Pb-Pb isochron approach with those published previously, the old values were recalculated using Isoplot, taking account of updated recommendations for decay constants (the following values were used in this comparison: $\lambda^{147}Sm = 6.54 \times 10^{-12}$ yr^{-1} – Lugmair and Marti, 1978; $\lambda^{87}Rb = 1.3972 \times 10^{-11}$ yr^{-1} – Villa et al., 2015; $\lambda^{40}K_{tot} = 5.5305 \times 10^{-10}$ yr^{-1} – Renne et al., 2010, 2011). A similar comparison for the ages presented in two previous studies (Snape et al., 2016b, 2018a) was made in those publications, although several of the recalculated literature ages have been updated here for consistency (in particular the Rb-Sr values), and are therefore highlighted in this discussion. The ages inferred from the Pb-Pb isochrons are generally in good agreement with those determined previously for the same samples, but several exceptions are discussed below (Figs. 7–9).

Some discrepancies are noted for two of the Apollo 11 samples. Firstly, the Pb-Pb isochron age of the Apollo 11 Group B3 high-Ti basalt, 10045, is older than the ^{40}Ar-^{39}Ar age from Geiss et al. (1977), although these authors note that the data for this sample did not yield a reliable ^{39}Ar release plateau, making the age determination questionable (Geiss et al., 1977; Guggisberg et al., 1979). Furthermore, the new 10045 age is similar to that of the other Group B3 basalt, 10020, analysed in this study. Notably, Tartèse et al. (2013) published Pb isotopic composi-

Please cite this article in press as: Snape J. F., et al. The timing of basaltic volcanism at the Apollo landing sites. *Geochim. Cosmochim. Acta* (2019), https://doi.org/10.1016/j.gca.2019.07.042

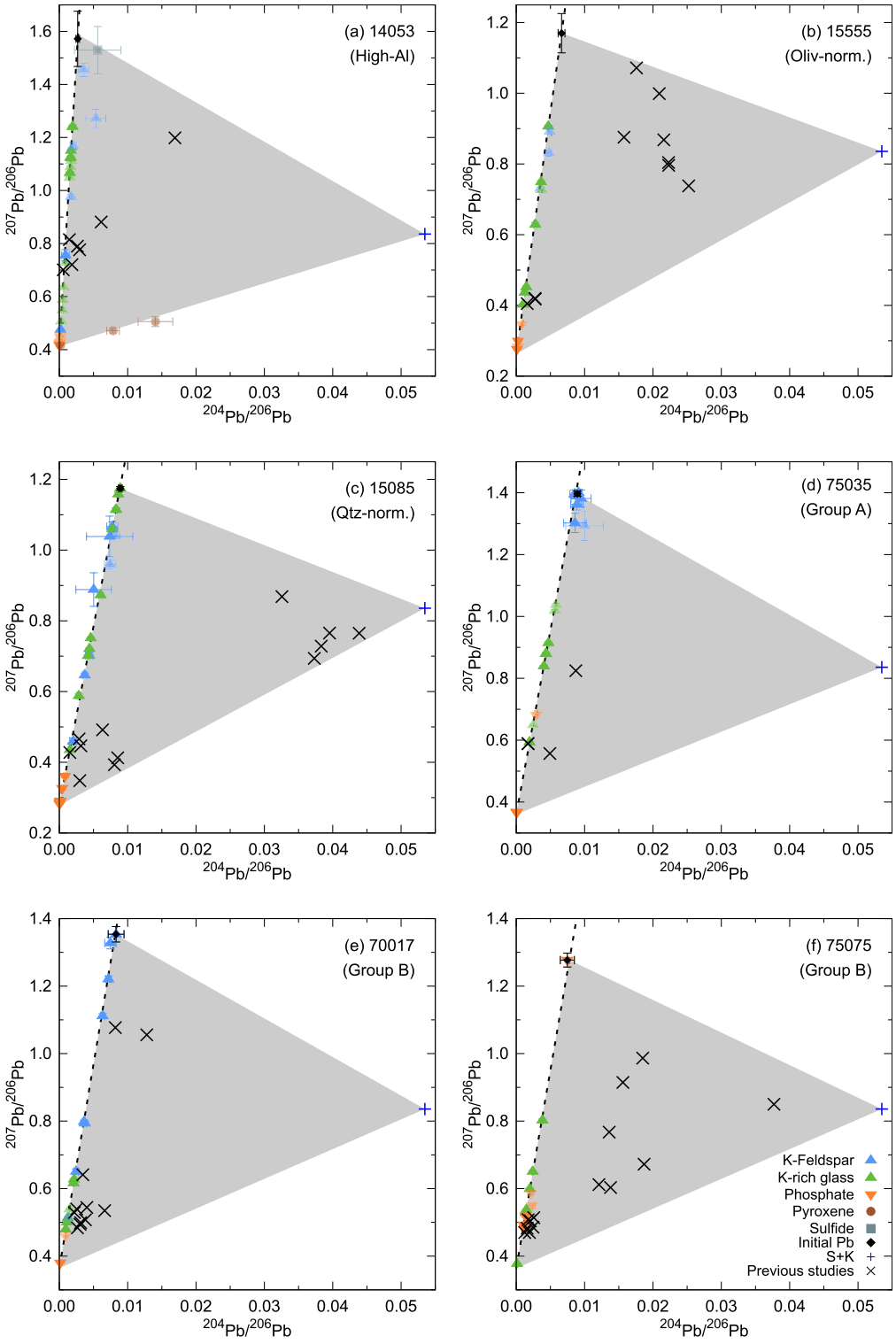

Fig. 6. Comparison of the Pb isotopic data obtained for several of the samples in this study with those presented previously. Data from the Apollo 14 high-Al basalt, 14053 (panel a), are compared with those collected by Tatsumo et al. (1972a) and Tera and Wasserburg (1972). Data from the two Apollo 15 basalts, 15555 and 15085 (panels b and c), are compared with those from Tatsumoto et al. (1972b), Tera and Wasserburg (1974) and Unruh and Tatsumoto (1977). Data from the three Apollo 17 basalts, 75035, 70017 and 75075 (panels d, e and f), are compared with those from Nunes et al. (1974), Tera and Wasserburg (1974), Mattinson et al. (1977) and Chen et al. (1978). In all cases, the data obtained in previous studies are consistent with the three component mixing relationship discussed in Section 2.3 and illustrated in Fig. 2, with the data lying to the right of the Pb-Pb isochrons for each sample and within the triangle defined by the isochron and a modern terrestrial Pb component (represented here with the model composition of modern terrestrial Pb presented by Stacey and Kramers (1975); "S + K").

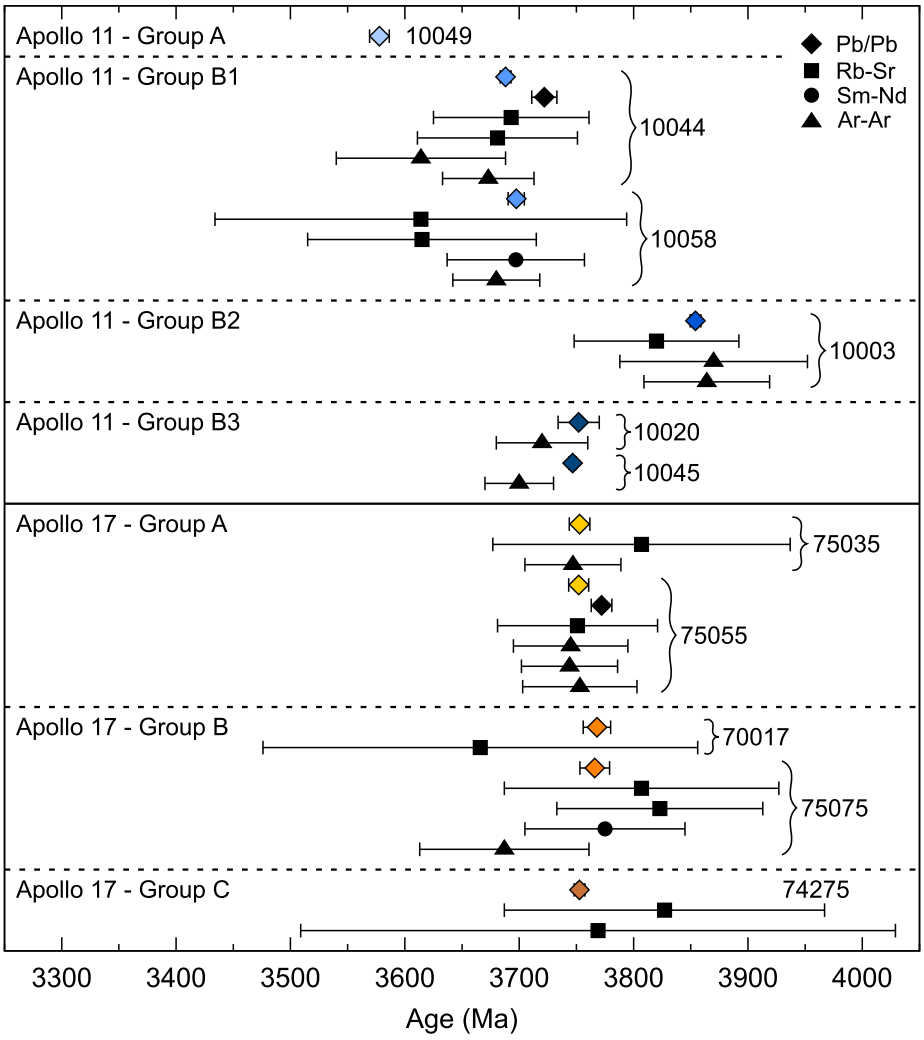

Fig. 7. Comparison of the Pb-Pb isochron ages for the high-Ti Apollo basalts with previous age determinations by other methods (see Table B.4. for a full list of references), which have been recalculated to account for updated decay constants. Error bars are scaled to represent the 95% confidence level.

tions of tranquillityite in the same section of 10044, which were used to calculate an older $^{207}Pb/^{206}Pb$ age of 3722 ± 11 Ma. As was discussed previously (Snape et al., 2016b), and similar to the case of the Apollo 17 sample 75055 (see Section 3), this older age can be explained by the lack of a correction for the effects of a lunar initial Pb component. Despite this, the individual analyses from the Tartèse et al. (2013) dataset are in good agreement with the isochron determined for that sample (Fig. 6 of Snape et al., 2016b).

The ages for the Apollo 12 samples 12002 (olivine basalt), 12021 (pigeonite basalt) and 12063 (ilmenite basalt) inferred from the Pb-Pb isochrons are younger than previous ages calculated from internal Rb-Sr isochrons comprising analyses of mineral separates (Papanastassiou and Wasserburg, 1970, 1971b; Murthy et al., 1971). In the case of 12021 and 12063, additional Rb-Sr isochron ages, reported by Cliff et al. (1971) and Papanastassiou and Wasserburg (1971b) are within error of the new crystallisation ages. Furthermore, the new age 12063 is consistent with the ages determined for the other ilmenite basalts using the Pb-Pb isochron approach. Two ^{40}Ar-^{39}Ar ages were reported for 12002 by Turner (1971) and Alexander (1972), both of which are within error of the age inferred from the 12002 Pb-Pb isochron. The new 12002 crystallisation age is also consistent with that determined for the olivine basalt 12012 (Fig. 8).

There are older Rb-Sr isochron ages for the Apollo 15 olivine-normative basalts 15016 and 15555, and the quartz-normative basalt 15058 (Fig. 8; Chappell et al., 1972; Birck et al., 1975; Snyder et al., 1998). For 15016, a Sm-Nd isochron age (Snyder et al., 1998), and an additional Rb-Sr isochron age determined by Evensen et al. (1973) are consistent with the age determined from the Pb-Pb isochron. In the case of 15555, Chappell et al. (1972) noted that their data were affected by variability in their Rb blank, which was subsequently cited as an explanation for the discrepancy of their age from the majority of those

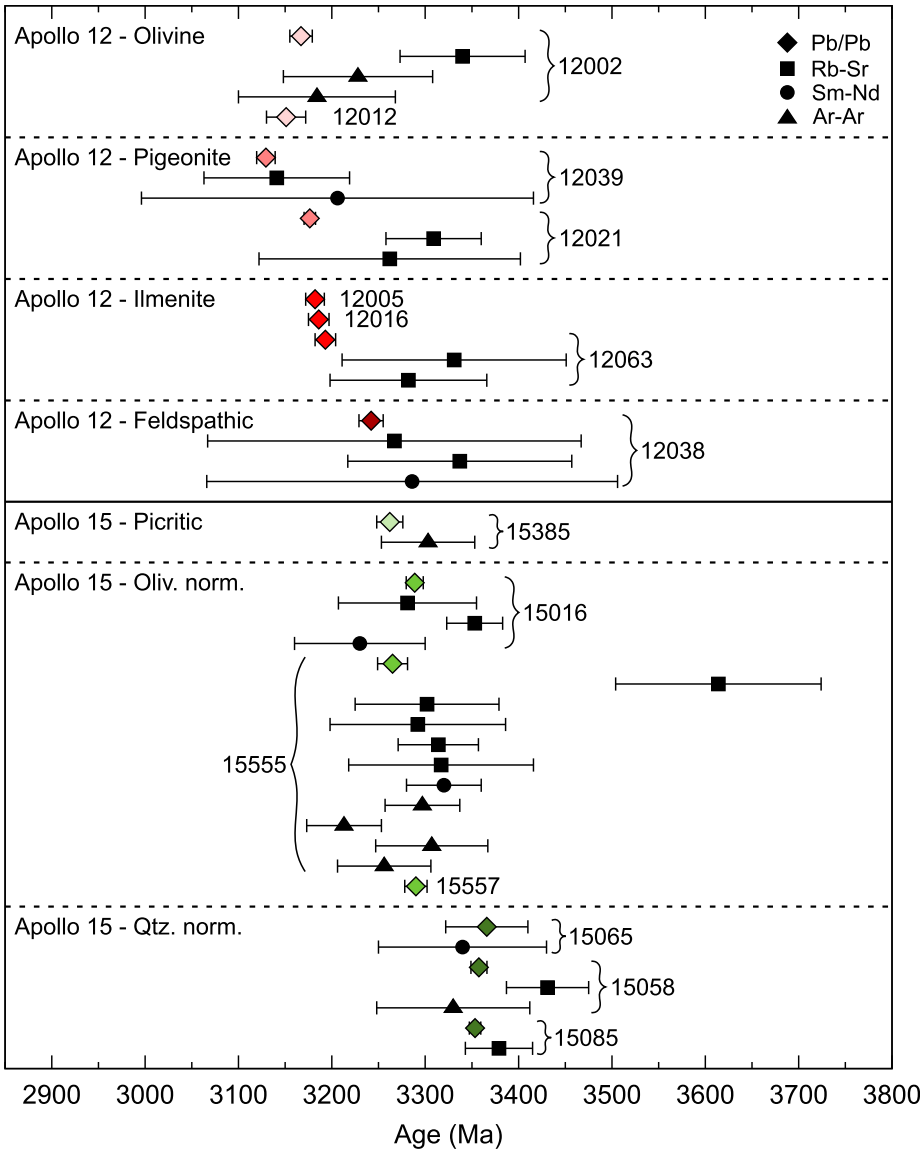

Fig. 8. Comparison of the Pb-Pb isochron ages for the low-Ti Apollo basalts with previous age determinations by other methods (see Table B.4. for a full list of references). The literature ages have been recalculated to account for updated decay constants and other factors (an exception being several of the ^{40}Ar-^{39}Ar ages, where there was not sufficient information to recalculate the monitor ages). Error bars are scaled to represent the 95% confidence level.

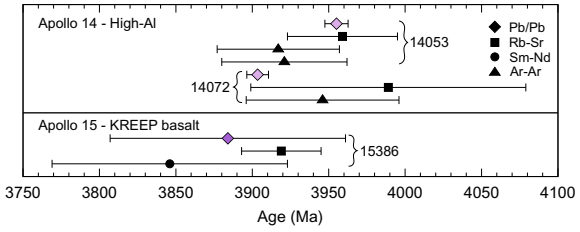

Fig. 9. Comparison of the Pb-Pb isochron ages for the Apollo 14 high-Al basalts and the Apollo 15 KREEP basalt, 15386, with previous age determinations by other methods (see Table B.4. for a full list of references), which have been recalculated to account for updated decay constants. Error bars are scaled to represent the 95% confidence level.

determined for the sample (Papanastassiou and Wasserburg, 1973). With this in mind, it is noted that the new age defined by the Pb-Pb isochron is in much better agreement with the younger ages determined by the other analyses of the 15555 basalt (Fig. 8). Finally, for the quartz-normative basalt, 15058, the Rb-Sr age determined by Birck et al. (1975) is only marginally outside of the uncertainties of the age determined from the Pb-Pb isochron. Furthermore, ^{40}Ar-^{39}Ar data obtained by Husain (1974) produce a well-defined plateau age of 3330 $\pm$ 80 Ma for 15058, consistent with the Pb-Pb isochron age for the sample.

4.3. Timing of volcanism at the Apollo landing sites

Several average age estimates have been presented previously for the different groups of Apollo basalts. As part of detailed discussions for basalts form specific landing sites, Paces et al. (1991) and Snyder et al. (1994) calculated weighted average ages for the Apollo 11 and 17 high-Ti basalts, while Snyder et al. (1997) presented weighted average values for the low-Ti Apollo 12 basalts. In addition to these, a more general overview of lunar chronology by Stöffler and Ryder (2001) included average ages for all of the major basalt groups. A number of differences are noted between the ages in these studies (Table 2), although the reasons for these are not completely clear, as only the Paces et al. (1991) and Snyder et al. (1994) studies explicitly state which samples age determinations were included in their calculations. In any case, in order to make a useful comparison with the Pb-Pb isochron ages, new weighted average values were calculated for this study using age determinations that were recalculated as described in Section 4.1 (a complete list of the samples and ages in these calculations is provided in Table B.5). Note, for the Apollo 11 and 17 high-Ti basalts, the same selection of age determinations were included as used previously (Paces et al., 1991; Snyder et al., 1994), and the values were simply updated to use a consistent set of decay constants (Lugmair and Marti, 1978; Villa et al., 2015; Renne et al., 2010, 2011).

4.3.1. Low-Ti basalts

The average ages calculated by Snyder et al. (1997) for the three main Apollo 12 basaltic suites (i.e. the ilmenite, olivine, and pigeonite basalts; e.g., Rhodes et al., 1977; Neal et al., 1994) were similar enough that they did not provide significant insight to the stratigraphic sequence of the Apollo 12 basalt flows, given the uncertainties on the original age determinations. The only potentially significantly different age was that of the feldspathic basalt, 12038, which had a weighted average age of 3280 Ma. The average ages presented by Stöffler and Ryder (2001) differ slightly, with a younger average age (3200 ± 80 Ma) for the feldspathic basalt, placing it within the uncertainties of the other three basaltic suites. The updated set of weighted average ages calculated for the Apollo 12 basalt suites in this study is closer to that of Snyder et al. (1997): pigeonite $= 3163 \pm 36$ Ma; olivine $= 3202 \pm 58$ Ma; ilmenite $= 3185 \pm 40$ Ma; feldspathic $= 3313 \pm 93$ Ma.

The ages presented by Snape et al. (2018a) for the Apollo 12 samples dated using the Pb-Pb isochron approach are in good agreement with these weighted average values (Table 1). These new ages also confirm the older age of the feldspathic basalt (3242 ± 13 Ma), as discussed by Snyder et al. (1997), indicating that the paucity of feldspathic basalts in the Apollo 12 sample collection may simply be due to the fact that the basalt flow is poorly represented on the surface due to its depth beneath the other flows in the region. Furthermore, the new ages make it possible to resolve differences between the timing of emplacement for the ilmenite, olivine and pigeonite basalts, resulting in a new stratigraphic sequence, with the ilmenite basalts being the oldest of the three main basaltic suites (3187 ± 6 Ma). This is followed by the pigeonite and olivine basalts, which have an age range constrained by the oldest and youngest pigeonite basalts; 3176 ± 6 Ma and 3129 ± 10 Ma, while the olivine basalts have an intermediate age of 3163 ± 10 Ma.

A more obvious chronological division between the two main groups of Apollo 15 low-Ti basalts (olivine-normative and quartz-normative) can be seen based on previous age determinations, which can be combined to provide weighted average ages of 3287 ± 21 Ma and 3371 ± 21 Ma for the Apollo 15 olivine-normative and quartz-normative basalts. By comparison, the picritic basalts have an average age of 3303 ± 50 Ma. The new Apollo 15 basalt ages, determined from Pb-Pb isochrons, are consistent with these weighted average ages (Table 2).

The picritic basalt, 15385, has the youngest age (3262 ± 14 Ma) of the Apollo 15 samples analysed here. The 8.7 g sample was collected together with a similar basaltic chip (15387; 2 g) as part of a rake sample on the rim of Spur crater. A compositionally similar basaltic clast was also identified in the breccia sample, 15459 (Hubbard et al., 1974; Nyquist et al., 1989), which was collected at the same location as the rake sample. Both of the basaltic chips, and the clast in 15459, have a high Mg content when compared to the other Apollo 15 basalts. Whereas the anomalous Apollo 12 feldspathic basalt, 12038, could potentially be explained by it originating from an underlying basalt flow that was poorly sampled due to its depth, this explanation does not fit with the Apollo 15 picritic basalts, due to the relatively young age of 15385. As such, it seems more likely these samples represent material that originated from a basalt flow near the Apollo 15 landing site that was introduced by an impact event. This could also provide an explanation for the incorporation of some basaltic material in the 15459 breccia.

4.3.2. High-Ti basalts

One clear difference between the Apollo 11 and 17 high-Ti basalts is the timespan over which they appear to have been emplaced. This was already clear with previous studies of the samples, with the weighted average ages of the Apollo 11 basalts varying from ~3600 to 3850 Ma, while the Apollo 17 basalts have a smaller range of ages, from ~3700 to 3800 Ma (Table 2). The new ages determined from the Pb-Pb isochrons for the samples confirm this difference in emplacement histories and make the comparison even more striking, with all of the Apollo 17 basalts having ages between 3740 and 3780 Ma, compared to the ~250 Ma period over which the Apollo 11 basalts were emplaced.

One notable discrepancy between the average ages for the Apollo 11 samples presented by Snyder et al. (1994) compared with those of Stöffler and Ryder (2001), is the distinction between the type B1 and B3 basalts. The recalculated weighted averages in Table 2 follow the Snyder et al. (1994) approach, with the B1 basalts having an average age of 3685 ± 18 Ma. Prior to the Pb-Pb isochrons

Please cite this article in press as: Snape J. F., et al. The timing of basaltic volcanism at the Apollo landing sites. *Geochim. Cosmochim. Acta* (2019), https://doi.org/10.1016/j.gca.2019.07.042

Table 2
Summary of the weighted average ages for the different groups of Apollo basalts. The original values presented by Paces et al. (1991), Snyder et al. (1994, 1997) and Stöffler and Ryder (2001) are included here for reference. These literature values have not been recalculated to correct for updated decay constants, due to the lack of information about which samples were included in some of these averages (although the revised average values for the Apollo 11 and 17 high-Ti basalts were generated using the age determinations specified by Paces et al. (1991) and Snyder et al. (1994)). The revised average values are based on age determinations that have been recalculated using the decay constants recommended by Lugmair and Marti (1978), Villa et al. (2015) and Renne et al. (2010, 2011). The values in bold are those proposed by Stöffler and Ryder as the best estimates for the surface flow ages, and the corresponding updated values (in the final columns). All uncertainties are stated at the 95% confidence level.

Landing site	Basalt group	Average ages (Ma)									
		Average of Pb-Pb isochron ages		Snyder et al. (1994, 1997)/Paces et al. (1991)		Stöffler and Ryder (2001)		Recalculated average (excluding Pb-Pb data)		Recalculated average (including Pb-Pb data)	
Apollo 11	High-Ti, Group A	3578	±9	3590	±40	**3580**	**±10**	**3588**	**±14**	**3580**	**±9**
Apollo 11	High-Ti, Group B1	3691	±4	3670	±20	3700	±20[§]	3685	±18	3691	±4
Apollo 11	High-Ti, Group B2	3854	±5	3850	±20	**3800**	**±20**	**3853**	**±51**	**3854**	**±8**
Apollo 11	High-Ti, Group B3	3747	±3	3710	±20	3700	±20[§]	3729	±30	3747	±3
Apollo 12	Low-Ti, Olivine	3163	±10	3190		3220	±40	3202	±58	3167	±18
Apollo 12	Low-Ti, Pigeonite (12039)*	3129	±10	3180		**3150**	**±40**	3163	±36	***3129***	***±10***
Apollo 12	Low-Ti, Pigeonite (12021)*	3176	±6	3180		**3150**	**±40**	3163	±36	*3176*	*±6*
Apollo 12	Low-Ti, Ilmenite	3187	±6	3200		3170	±20	3187	±43	3187	±11
Apollo 12	Low-Ti, Feldspathic	3242	±13	3280		3200	±80	3313	±93	3243	±13
Apollo 14	High-Al (14053)*	3955	±8	-		-		3934	±60	*3955*	*±8*
Apollo 14	High-Al (14072)*	3905	±8	-		-		3956	±43	*3905*	*±8*
Apollo 15	KREEP	3884	±77	-		-		3889	±29	3889	±24
Apollo 15	Low-Ti, Picritic	3262	±14	-		3250	±50	3303	±50	3265	±13
Apollo 15	Low-Ti, Olivine normative	3285	±7	-		**3300**	**±20**	**3287**	**±21**	**3285**	**±9**
Apollo 15	Low-Ti, Quartz normative/ pigeonite	3356	±6	-		3350	±10	3371	±21	3357	±7
Apollo 17	High-Ti, Group A	3752	±7	3750	±20	**3750**	**±10**	**3761**	**±13**	**3754**	**±6**
Apollo 17	High-Ti, Group B	3767	±9	3690	±20	3700	±20	3732	±40	3764	±12
Apollo 17	High-Ti, Group C	3753	±5	3722	±67	**3750**	**±70**	**3791**	**±58**	**3753**	**±5**

* The ages determined from the Pb-Pb isochrons for the Apollo 12 pigeonite and Apollo 14 high-Al basalts indicate that they were formed by separate eruptions. As such, weighted average values incorporating the new Pb-Pb isochron ages were not recalculated for these basaltic groups and the individual sample ages are assumed instead (in italics in the final column).
§ Stöffler and Ryder (2001) provided a combined average age for the B1 and B3 basalts.

Please cite this article in press as: Snape J. F., et al. The timing of basaltic volcanism at the Apollo landing sites. *Geochim. Cosmochim. Acta* (2019), https://doi.org/10.1016/j.gca.2019.07.042

presented here, the only age determinations for any of the B3 basalts originated from the ^{40}Ar-^{39}Ar analyses of Geiss et al. (1977) and Guggisberg et al. (1979), of which only one (for the 10050 basalt) yielded a reliable high-temperature release plateau of 3729 ± 30 Ma. The Pb isotopic data are in good agreement with these ages, and confirm the distinction between the two groups (Table 2).

Compared with that of the Apollo 11 basalts, the relatively brief ~40 Ma period of mare volcanism sampled by the Apollo 17 basalts makes it difficult to confidently resolve any chronological distinctions between the different Apollo 17 basaltic groups. Based on the two samples analysed here, the Group B basalts (3767 ± 9 Ma), may be slightly older than either the Group A (3752 ± 7 Ma) or Group C (3753 ± 5 Ma) basalts (Table 2).

4.3.3. High-Al and KREEP basalts

Previous ^{40}Ar-^{39}Ar, Rb-Sr and Sm-Nd analyses of the 15382 and 15386 KREEP basalts (Turner et al., 1973; Stettler et al., 1973; Nyquist et al., 1975; Carlson and Lugmair, 1979) can be combined to yield a weighted average age of 3889 ± 29 Ma. Adding the new Pb-Pb isochron age of 15386 to this average results in an identical age of 3889 ± 24 Ma. The Apollo 15 KREEP basalts have previously been interpreted as representing samples of the light plains unit within the Imbrium basin, referred to as the Apennine Bench Formation (ABF; Hawke and Head, 1978; Spudis, 1978; Ryder, 1994; Taylor et al., 2012). This unit is generally accepted to have been emplaced after the formation of the Imbrium basin (Taylor et al., 2012), although Deutsch and Stöffler (1987) proposed that it could represent a pre-existing unit exposed within the basin. Furthermore, it has also been suggested that the formation of the Apollo 15 KREEP basalts could have been triggered by the formation of the Imbrium impact basin (Ryder, 1994; Taylor et al., 2012). Previous younger estimates for the age of the Imbrium basin (3850 Ma or younger; Stöffler and Ryder, 2001 and references therein) would challenge the interpretation that the samples represented material from the ABF and post-dated the formation of the basin. By contrast, more recent U-Pb analyses of Ca-phosphates in breccias from multiple Apollo landing sites indicate that the basin was formed at ~3920 Ma (Snape et al., 2016a; Thiessen et al., 2017, 2018), consistent with the Apollo 15 KREEP basalts forming subsequently as part of the ABF.

Ages determined by ^{40}Ar-^{39}Ar and Rb-Sr analyses of the Apollo 14 high-Al basalts, 14053 (Papanastassiou and Wasserburg, 1971a; Turner et al., 1973; Stettler et al., 1973) and 14072 (Compston et al., 1972; York et al., 1972), indicated that both could potentially have a similar age of 3939 ± 20 Ma. Conversely, with the benefit of the smaller uncertainties associated with the new Pb isochron ages, it now appears that the two basalts originate from flows emplaced at distinct times (14053 = 3955 ± 8 Ma; 14072 = 3905 ± 8 Ma; Table 1 and Fig. 9) separated by between 35 and 65 Ma. Notably, and by contrast with the Apollo 15 KREEP basalts, the ages of the Apollo 14 basalts indicate that this form of high-Al volcanism was occurring before and up until (potentially even after) the formation of the Imbrium basin.

4.4. Lead isotope systematics of the Apollo basalts

4.4.1. Constraining initial Pb isotopic compositions

The focus of this study has primarily been to review the chronological implications of these Pb isotopic data, but the initial Pb isotopic compositions estimated for each of the samples can provide additional insights into the evolving nature of the mare basalts (e.g., Snape et al., 2018a) and the magmatic evolution of the Moon in general (e.g., Snape et al., 2016b). A caveat to this is the confidence with which the initial Pb isotopic compositions have been determined and the potential for having underestimated these values. In other words, the values on a given sample isochron with the highest ^{204}Pb/^{206}Pb and ^{207}Pb/^{206}Pb may not represent the "pure" initial Pb component, but may contain some proportion of Pb generated by the radiogenic decay of U after the sample crystallised. Given the steepness of the sample isochrons (with slopes of approximately 100 for some of the mare basalts, and increasing to nearly 600 for the Apollo 15 KREEP basalt, 15386), such underestimations will affect the initial ^{207}Pb/^{206}Pb ratios more dramatically than the ^{204}Pb/^{206}Pb ratios.

Previously, it was suggested that the most confident initial Pb determinations came from the samples where these compositions are defined by multiple analyses, particularly in K-feldspar and plagioclase phases, where there are lower concentrations of U than in many of the analysed K-rich glass areas (Snape et al., 2016b, 2018a). An additional check of these values can potentially be made using the alternative approach for estimating the isotopic composition of the initial Pb component (discussed in Section 3), where the mixing line between the initial Pb component and the contaminant is defined and the intercept between this and the sample isochron is calculated. This approach is only effective when there are sufficient points to define this mixing line (such as with the datasets from the two Apollo 15 samples in Fig. 2). A third alternative (used in both Snape et al., 2016b, 2018a), is to calculate "predicted" initial Pb isotopic compositions based on a given model for Pb isotopic evolution in the Moon, by calculating paleoisochrons using an assumed starting composition and time, and identifying where these intersect the sample isochrons. The obvious problem with this approach is that such predicted values are highly model-dependent.

4.4.2. New constraints for the mare basalt mantle sources

Despite the uncertainties in the initial Pb isotopic compositions, a preliminary observation is that the younger basaltic groups for both the high-Ti mare basalts (the Apollo 11 Group A samples) and the low-Ti mare basalts (the Apollo 12 olivine and pigeonite basalts) cannot be explained simply by continued evolution of the same mantle sources from which the older basalts originated (the Apollo 11 Group B2 sample and the Apollo 15 quartz normative; Fig. 10). Instead the isotopic compositions of these younger groups would require either: (1) the existence of multiple distinct mantle sources with higher ^{238}U/^{204}Pb ratios (μ-

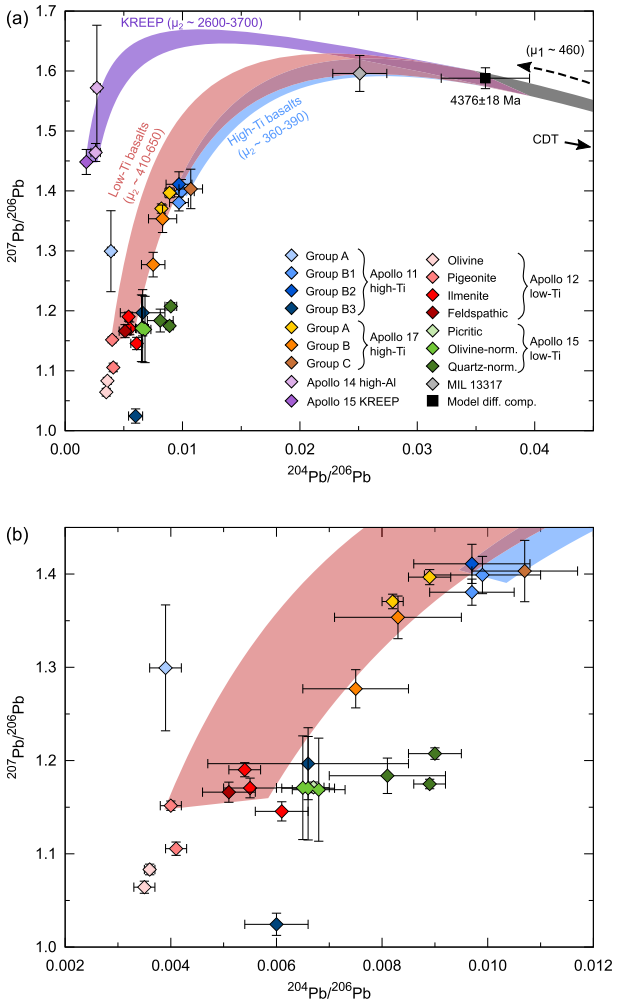

Fig. 10. (a) $^{207}Pb/^{206}Pb$ vs. $^{204}Pb/^{206}Pb$ plots of the initial Pb compositions of the Apollo basalts analysed in this and two previous studies (Snape et al., 2016b, 2018a). The data are compared with the initial Pb isotopic composition of ancient basaltic clasts in the lunar meteorite MIL 13317 (Snape et al., 2018b) and the multiple stage Pb isotopic evolution model of Snape et al. (2016b). The model is calculated assuming lunar formation at 4500 Ma and a primitive starting composition of Canyon Diablo Troilite (CDT; Göpel et al., 1985). In the model, an undifferentiated bulk Moon with a μ_1-value of ~460 evolves until 4376 ± 18 Ma, after which, the mantle sources of the Apollo basalts are modelled as originating from the model differentiation composition with distinct μ_2-values. (b) Focusing just on the low-Ti and high-Ti basalts, it is clear that from the expanded data set presented here that a wider range of μ_2-values than was described in the original model would be necessary to explain the full array of initial Pb isotopic compositions.

values) than those of the older groups; or (2) mixing with larger proportions of high-μ material, such as the sources of the KREEP basalts. For example, the fairly narrow range of μ-values previously estimated for the low-Ti and high-Ti basalt sources (Snape et al., 2016b) would not be sufficient to explain the wider range of initial Pb compositions in this expanded dataset (Fig. 10). The requirement for higher μ sources of the younger basalts or mixing with high-μ material can be seen more clearly when the initial $^{206}Pb/^{204}Pb$ compositions are plotted against the crystallisation ages (Fig. 11). This relationship is most apparent in the low-Ti mare basalts (Fig. 11b), although the scatter in high-Ti basalt values may reflect underestimations of the initial Pb isotopic compositions.

Even within the different basalts collected at individual landing sites, the differences between the Pb isotopic compositions of the samples are significant enough to require multiple mantle sources or varying degrees of mixing with high-μ material. In the case of Apollo 12, the three main basalt suites can be modelled as a mixture between a primitive mafic cumulate and a KREEP-rich component, with the ilmenite basalt source having less KREEP-rich material than the pigeonite and olivine basalt sources (Snyder et al., 1997; Hallis et al., 2014; Snape et al., 2018a). This relationship also appears to be consistent for the Rb-Sr and Sm-Nd isotope systems (Snyder et al., 1997; Snape et al., 2018a).

In the case of the Apollo 15 low-Ti basalts, the olivine-normative basalts and the picritic basalt (15385) have Pb isotopic compositions that are similar enough to be explained by a common mantle source, while the quartz-normative basalts originated from a lower μ source (Fig. 11), potentially consistent with earlier interpretations of these basalts (Rhodes and Hubbard, 1973; Snyder et al., 2000). This is in contrast to the model presented by Schnare et al. (2008), in which a common mantle source is assumed for the olivine- and quartz-normative basalts, with the compositions of the basalts being explained by varying degrees of fractionation occurring either at crustal levels in magma chambers and dikes, or near the surface in lava flows. In order to explain the data presented here, the olivine- and quartz-normative basalt sources either need to have evolved completely separately to allow for sufficient evolution of the Pb isotopic compositions or, alternatively, the olivine-normative basalt (and picritic basalt) source would need to have incorporated more high-μ material from another source.

The combined set of Pb isotopic data from all of the low-Ti basalts indicates that the Apollo 12 basalt sources either had higher μ values or incorporated larger amounts of high-μ material than the Apollo 15 sources. However, a complication arises when looking at Lu-Hf and Sm-Nd systematics, which indicate that there was less KREEP mixed into the Apollo 12 sources than those of the Apollo 15 basalts (Sprung et al., 2013). This suggests mixing between similar primitive mafic cumulates and KREEP-rich sources alone cannot explain the range of μ-values in the Apollo 12 and 15 low-Ti basalts.

Previous models for sources of the Apollo 11 high-Ti basalts (Snyder et al., 1994) also proposed varying amounts of late-stage Lunar Magma Ocean (LMO) residual melt mixing with the more primitive partial melts of the lunar mantle cumulates. This mixing is potentially consistent with the second hypothesis proposed above, although in order to test these models with the Pb isotopic compositions, it will be necessary to more confidently constrain the initial Pb compositions of the samples, particularly for the high-Ti basalts. This could potentially be achieved with further

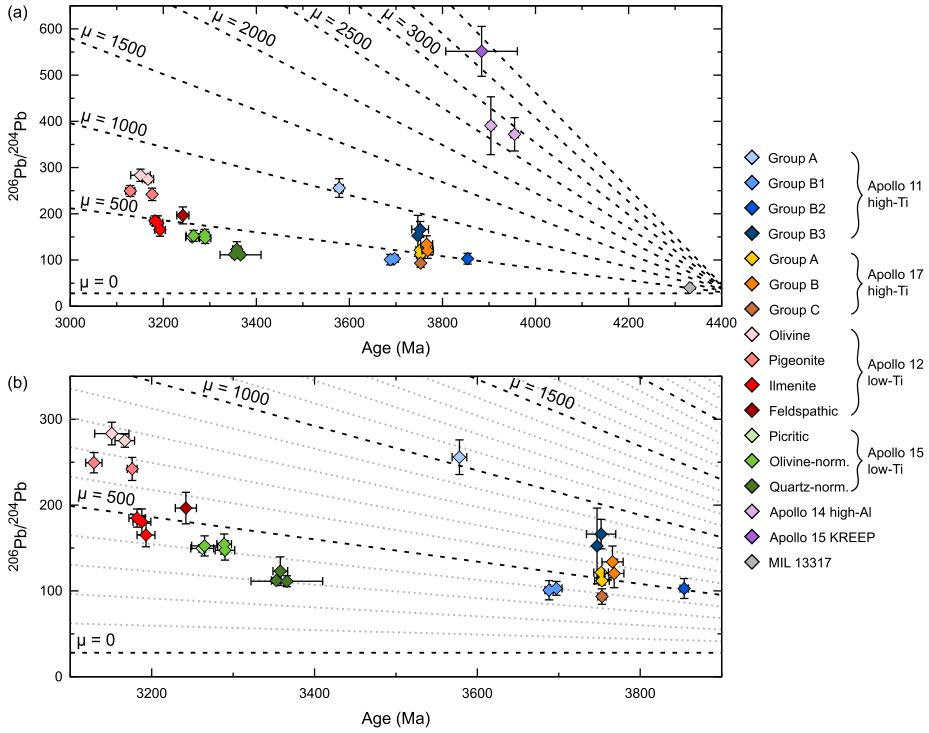

Fig. 11. (a) Initial $^{206}Pb/^{204}Pb$ ratios of the Apollo basalts plotted against the crystallisation ages. The dashed lines represent the evolution of mantle sources at a given μ-value (starting from the model differentiation composition and time presented by Snape et al., 2016b). (b) Focusing on the low-Ti and high-Ti mare basalts, there is a broad trend towards higher μ-values in the younger samples.

SIMS analyses, focusing on K-feldspar and plagioclase phases. It may also be helpful to complement these datasets with new thermal ionisation mass spectrometry (TIMS) measurements of plagioclase grains. Following on from this, it would also be interesting to test the proposed genetic link between the Apollo 11 Group B2 basalts and the similarly aged, but chemically anomalous, basaltic soil fragments from the same landing site, classified as a separate basaltic group (Group D), based on their higher concentrations of incompatible trace elements and potential enrichment of KREEP-like material (Beaty et al., 1979; Snyder et al., 1996).

4.5. Implications for crater counting studies

Stöffler and Ryder (2001) reviewed the age determinations for Apollo basalts available at the time, in order to determine which particular basalts provided the best estimate for the ages of surface flows at each landing site (these have been highlighted in Table 2). That analysis is still widely cited in studies determining the absolute ages of geologic units on the Moon from crater frequency statistics (e.g., Hiesinger et al., 2010; Robbins, 2014; Fassett, 2016). As such, the new Pb-Pb isochron ages presented in this study have been assessed in relation to the Stöffler and Ryder (2001) discussion.

The most obvious difference is with the Apollo 11 Group B2 ages that are approximately 50 Ma older than the 3800 Ma age presented by Stöffler and Ryder (2001). This includes both the recalculation of previous age determinations (i.e. without incorporating the Pb-Pb isochron ages), and the averages incorporating the new crystallisation ages presented in this study (Table 2). For all other surface flow ages, the values presented by Stöffler and Ryder (2001) are within error of the new average ages, even when taking into account the smaller uncertainties that result from including the new Pb-Pb isochron ages.

One particularly important outcome of previous crater size-frequency distribution measurements was the identification of mare basalt flows significantly younger than those visited by the Apollo or Luna missions, with estimated ages of ~1200 Ma (Hiesinger et al., 2003). Current plans of the Chinese National Space Administration (CNSA) for its Chang'E-5 mission involve returning samples from the Mons Rümker region of Oceanus Procellarum, near to these young mare basalt flows (Qian et al., 2018). The ability to accurately and precisely determine the ages basalts returned from this mission will be vital in order to assess the accuracy of the ages estimated by Hiesinger et al. (2003), but more importantly to better calibrate the crater production functions used to translate crater counting statistics of planetary surfaces into absolute age estimates.

5. CONCLUSIONS

The Pb isotope data presented in this study for a range of Apollo basalts, have been used to constrain crystallisation ages, which are good agreement with previous estimates for the timing of lunar mare volcanism at the Apollo landing sites. The smaller uncertainties associated with this technique make it possible to resolve differences in the crystallisation ages between the various basaltic

Please cite this article in press as: Snape J. F., et al. The timing of basaltic volcanism at the Apollo landing sites. *Geochim. Cosmochim. Acta* (2019), https://doi.org/10.1016/j.gca.2019.07.042

groups sampled at each of the landing sites. For example, the data confirm the old age of the Apollo 14 high-Al basalts, relative to the high-Ti and low-Ti mare basalts, and indicate that the high-Al basalts were emplaced in distinct events at 3955 ± 8 Ma and 3905 ± 8 Ma. The Apollo 15 KREEP basalts were being formed at a similar, potentially slightly later time of 3889 ± 24 Ma. These were followed by the emplacement of the first high-Ti mare basalts at the Apollo 11 site (the Group B2 samples at 3854 ± 8 Ma), and then subsequent high-Ti mare basalts at both the Apollo 11 and 17 landing sites around 3750 Ma. The final period of high-Ti mare volcanism sampled by the Apollo missions resulted in the emplacement of the Group A Apollo 11 basalts at 3580 ± 4 Ma. The earliest low-Ti mare volcanism sampled by the Apollo missions produced the Apollo 15 quartz-normative basalts at around 3357 ± 7 Ma. This was then followed by the formation of Apollo 15 olivine-normative basalts at 3285 ± 9 Ma and the picritic basalts at 3265 ± 13 Ma. Finally, low-Ti volcanism in the region of the Apollo 12 landing site basalts appears to have begun with the feldspathic basalt (12038) at 3243 ± 13 Ma, and concluded with the youngest of the pigeonite basalts (12039) at 3129 ± 10 Ma.

In addition to the crystallisation ages of the basalts, the Pb isotopic data have been used to estimate the composition of the initial Pb component in the different basalts. In many cases, these compositions appear to indicate a systematic increase in the radiogenic nature of basalt sources with time, which cannot be explained with the evolution of a single mantle source, although further analyses (particular for the high-Ti basalts) are necessary to confirm this observation.

Reviewing these results in light of previous studies demonstrates the reliability and potential of this approach for dating lunar basalts, which has already begun to contribute towards a more complete picture of the magmatic evolution of the Moon (Snape et al., 2016b, 2018a, 2018b). The development of this approach is particularly timely, given current plans of the CNSA for its Chang'E-5 mission. This aims to return samples from a location near some of the youngest mare basalt flows on the Moon (Hiesinger et al., 2003, 2010; Qian et al., 2018), which would be perfect candidates for the type of Pb isotopic analyses demonstrated in this study.

ACKNOWLEDGEMENTS

The authors thank the Apollo astronauts for collecting the samples analysed in this study, and all those who helped make the missions possible. This manuscript benefitted greatly from the editorial guidance of Dr. James Day and the detailed comments of three anonymous referees. The authors also thank Linda Chappell at the Lunar and Planetary Institute library for kindly supplying copies of various publications that made it possible to recalculate many of the old basalt ages in the literature. This work was funded by grants from the Knut and Alice Wallenberg Foundation (2012.0097) and the Swedish Research Council (VR 2012-4370 and 2017-4151) to MJW and AAN. Additionally, JFS acknowledges funding from the European Commission Horizon 2020 Research and Innovation programme, through a Marie Skłodowska-Curie Actions Fellowship grant (794287), and MA acknowledges funding from Science and Technology Facilities Council (STFC) grants (#ST/L000776/1 and #ST/P000657/1). During acquisition of data for this study, the NordSIMS facility was primarily funded by Swedish Research Council infrastructure grants 2014-6375 and 2017-00617, with additional support from the University of Iceland and the Swedish Museum of Natural History; this is NordSIMS publication #605. This research has made use of NASA's Astrophysics Data System.

APPENDIX A. SUPPLEMENTARY MATERIAL

Supplementary data to this article can be found online at https://doi.org/10.1016/j.gca.2019.07.042.

REFERENCES

Alexander E. C., Davis P. K. and Reynolds J. H. (1972) Rare-gas analyses on neutron irradiated Apollo 12 samples. Lunar Planet. Sci. III. Lunar Planet. Inst., Houston. pp. 1787–1795.

Beaty D. W. and Albee A. L. (1978) Comparative petrology and possible genetic relations among the Apollo 11 basalts. Lunar Planet. Sci. IX. Lunar Planet. Inst., Houston. pp. 359–463.

Beaty D. W., Hill S. M., Albee A. L., Ma M.–S. and Schmitt R. A. (1979) The petrology and chemistry of basaltic fragments from the Apollo 11 soil – I. Lunar Planet. Sci. X. Lunar Planet. Inst., Houston. pp. 41–75.

Bellucci J. J., Nemchin A. A., Whitehouse M. J., Humayun M., Hewins R. and Zanda B. (2015) Pb-isotopic evidence for an early, enriched crust on Mars. *Earth Planet. Sci. Lett.* **410**, 34–41. https://doi.org/10.1016/j.epsl.2014.11.018.

Birck J. L., Fourcade S. and Allegre C. J. (1975) $^{87}Rb/^{86}Sr$ age of rocks from the Apollo 15 landing site and significance of internal isochrons. *Earth Planet. Sci. Lett.* **26**, 29–35. https://doi.org/10.1016/0012-821X(75)90174-0.

Blundy J. and Wood B. (2003) Mineral-melt partitioning of uranium, thorium and their daughters. *Rev. Min. Geochem.* **52**, 59–123. https://doi.org/10.2113/0520059.

Brown G. M., Emeleus C. H., Holland J. G., Peckett A. and Phillips R. (1972) Mineral-chemical variations in Apollo 14 and Apollo 15 basalts and granitic fractions. Lunar Planet. Sci. III. Lunar Planet. Inst., Houston. pp. 141–157.

Brown G. M., Peckett A., Emeleus C. H., Phillips R. and Pinsent R. H. (1975) Petrology and mineralogy of Apollo 17 mare basalts. Lunar Planet. Sci. VI. Lunar Planet. Inst., Houston. pp. 1–13.

Butler P. (1971) Lunar Sample Information Catalog, Apollo 15. National Aeronautics and Space Administration, MSC 03209.

Carlson R. W. and Lugmair G. W. (1979) Sm-Nd constraints on early lunar differentiation and the evolution of KREEP. *Earth Planet. Sci. Lett.* **45**, 123–132. https://doi.org/10.1016/0012-821X(79)90114-6.

Chappell B. W., Compston W., Green D. H. and Ware N. G. (1972) Chemistry, geochronology, and petrogenesis of lunar sample 15555. *Science* **175**, 415–416. https://doi.org/10.1126/science.175.4020.415.

Chen J. H., Tilton G. R., Mattinson J. M. and Vidal P. (1978) Lead isotope systematics of mare basalt 75075. Lunar Planet. Sci. IX. Lunar Planet. Inst., Houston. pp. 509–521.

Cliff R. A., Lee-Hu C. and Wetherill G. W. (1971) Rb-Sr and U-Th-Pb measurements on Apollo 12 material. Lunar Planet. Sci. II. Lunar Planet. Inst., Houston. pp. 1493–1502.

Compston W., Vernon M. J., Berry H., Rudowski R., Gray C. M. and Ware N. (1972) Apollo 14 mineral ages and the thermal

history of the Fra Mauro formation. Lunar Planet. Sci. III. Lunar Planet. Inst., Houston. pp. 1487–1501.

Deutsch A. and Stöffler D. (1987) Rb-Sr-analyses of Apollo 16 melt rocks and a new age estimate for the Imbrium basin: Lunar basin chronology and the early heavy bombardment of the moon. *Geochim. Cosmochim. Acta* **51**, 1951–1964. https://doi.org/10.1016/0016-7037(87)90184-0.

Dowty E., Prinz M. and Keil K. (1973) Composition, mineralogy, and petrology of 28 mare basalts from Apollo 15 rake samples. Lunar Planet. Sci. IV. Lunar Planet. Inst., Houston. pp. 423–444.

Evensen N. M., Murthy V. R., and Coscio M. R. (1973) Rb-Sr ages of some mare basalts and the isotopic and trace element systematics in lunar fines. Lunar Planet. Sci. IV. Lunar Planet. Inst., Houston. pp. 1707–1724.

Fassett C. I. (2016) Analysis of impact crater populations and the geochronology of planetary surfaces in the inner solar system. *J. Geophys. Res. (Planets)* **121**, 1900–1926. https://doi.org/10.1002/2016JE005094.

Gancarz A. J., Albee A. L. and Chodos A. A. (1971) Petrologic and mineralogic investigation of some crystalline rocks returned by the Apollo 14 mission. *Earth Planet. Sci. Lett.* **12**, 1–18. https://doi.org/10.1016/0012-821X(71)90050-1.

Geiss J., Eberhardt P., Grögler N., Guggisberg S., Maurer P. and Stettler A. (1977) Absolute time scale of lunar mare formation and filling. *Phil. Trans. Royal Soc.* **285**, 151–158. https://doi.org/10.1098/rsta.1977.0051.

Grange M. L., Nemchin A. A., Pidgeon R. T., Timms N., Muhling J. R. and Kennedy A. K. (2009) Thermal history recorded by the Apollo 17 impact melt breccia 73217. *Geochim. Cosmochim. Acta* **73**, 3093–3107. https://doi.org/10.1016/j.gca.2009.02.032.

Grange M. L., Pidgeon R. T., Nemchin A. A., Timms N. and Meyer C. (2013) Interpreting U-Pb data from primary and secondary features in lunar zircon. *Geochim. Cosmochim. Acta* **101**, 112–132. https://doi.org/10.1016/j.gca.2012.10.013.

Guggisberg S., Eberhardt P., Geiss J., Grögler N., Stettler A., Brown G. M. and Peckett A. (1979) *Classification of the Apollo-11 mare basalts according to 40Ar-39Ar ages and petrological properties*. Houston, Lunar Planet. Sci. X. Lunar Planet. Inst., pp. 1–39.

Göpel C., Manhès G. and Allègre C. J. (1985) U-Pb systematics in iron meteorites - Uniformity of primordial lead. *Geochim. Cosmochim. Acta* **49**, 1681–1695. https://doi.org/10.1016/0016-7037(85)90139-5.

Hallis L., Anand M. and Strekopytov S. (2014) Trace-element modelling of mare basalt parental melts: Implications for a heterogeneous lunar mantle. *Geochim. Cosmochim. Acta* **134**, 289–316. https://doi.org/10.1016/j.gca.2014.01.012.

Hawke B. R. and Head J. W. (1978) Lunar KREEP volcanism - Geologic evidence for history and mode of emplacement. Lunar Planet. Sci. IX. Lunar Planet. Inst., Houston. pp. 3285–3309.

Hiesinger H., Head J. W., Wolf U., Jaumann R. and Neukum G. (2003) Ages and stratigraphy of mare basalts in Oceanus Procellarum, Mare Nubium, Mare Cognitum, and Mare Insularum. *J. Geophys. Res. (Planets)* **108**, 5065. https://doi.org/10.1029/2002JE001985.

Hiesinger H., Head J. W., Wolf U., Jaumann R. and Neukum G. (2010) Ages and stratigraphy of lunar mare basalts in Mare Frigoris and other nearside maria based on crater size-frequency distribution measurements. *J. Geophys. Res. (Planets)* **115**, E03003. https://doi.org/10.1029/2009JE003380.

Hubbard N. J., Shih C.–Y., Rhodes J. M., Wiesmann H. and Bansal B. M. (1974) The chemical definition and interpretation of rock types returned from the non-mare regions of the Moon. Lunar Planet. Sci. V. Lunar Planet. Inst., Houston. pp. 1227–1246.

Husain L. (1974) ^{40}Ar-^{39}Ar chronology and cosmic ray exposure ages of the Apollo 15 samples. *J. Geophys. Res.* **79**, 2588–2606. https://doi.org/10.1029/JB079i017p02588.

Jerde E. A., Snyder G. A., Taylor L. A., Liu Y. G. and Schmitt R. A. (1994) The origin and evolution of lunar high-Ti basalts - Periodic melting of a single source at Mare Tranquillitatis. *Geochim. Cosmochim. Acta* **58**, 515–527. https://doi.org/10.1016/0016-7037(94)90480-4.

Joy K. H. and Arai T. (2013) Lunar meteorites: new insights into the geological history of the Moon. *Astron. Geophys.* **54**, 4.28-4.32. https://doi.org/10.1093/astrogeo/att121.

Kushiro I., Ikeda Y. and Nakamura Y. (1972) Petrology of Apollo 14 high-alumina basalt. Lunar Planet. Sci. III. Lunar Planet. Inst., Houston. pp. 115–129.

Longhi J., Walker D., Stolper E. N., Grove T. L. and Hays J. F. (1972) Petrology of mare/rille basalts 15555 and 15065. In *The Apollo 15 Lunar Samples*. Lunar Planet. Inst, Houston, pp. 131–134.

Ludwig K. R. (2008) User's Manual for Isoplot 3.60, A geochronological toolkit for Microsoft Excel. Berkeley Geochronological Center Special Publication 4, Berkeley, California: Berkeley Geochronological Center.

Lugmair G. W. and Marti K. (1978) Lunar initial ^{143}Nd/^{144}Nd: differential evolution of the lunar crust and mantle. *Earth Planet. Sci. Lett.* **39**, 349–357. https://doi.org/10.1016/0012-821X(78)90021-3.

Mattinson J. M., Tilton G. R., Todt W., Chen J. H. and Merril R. B. (1977) *Lead isotope studies of mare basalt 70017*. Lunar Planet. Sci. VIII. Lunar Planet. Inst, Houston, pp. 1473–1487.

McGee P. E., Warner J. L. and Simonds C. H. (1977) Introduction to the Apollo Collections. Part 1: Lunar Igneous Rocks. National Aeronautics and Space Administration Technical Report #19770015090.

Merle R., Nemchin A., Grange M., Whitehouse M. and Pidgeon R. T. (2014) High-resolution U-Pb Ca-phosphate ages in Apollo 14 breccias: implications for the age of the Imbrium impact. *Meteorit. Planet. Sci.* **49**, 2241–2251. https://doi.org/10.1111/maps.12395.

Merle R. E., Nemchin A. A., Whitehouse M. J., Pidgeon R. T., Grange M. L., Snape J. F. and Thiessen F. (2017) Origin and transportation history of lunar breccia 14311. *Meteorit. Planet. Sci.* **52**, 842–858. https://doi.org/10.1111/maps.12835.

Murthy V., Evensen N., Jahn B.-M. and Coscio M. R. (1971) Rb-Sr ages and elemental abundances of K, Rb, Sr, and Ba in samples from the Ocean of Storms. *Geochim. Cosmochim. Acta* **35**, 1139–1153. https://doi.org/10.1016/0016-7037(71)90030-5.

Neal C. R., Taylor L. A., Hughes S. S. and Schmitt R. A. (1990) The significance of fractional crystallization in the petrogenesis of Apollo 17 Type A and B high-Ti basalts. *Geochim. Cosmochim. Acta* **54**, 1817–1833. https://doi.org/10.1016/0016-7037(71)90030-5.

Neal C. R., Hacker M. D., Snyder G. A., Taylor L. A., Liu Y. G. and Schmitt R. A. (1994) Basalt Generation at the Apollo 12 Site, Part 1: New Data. *Classification, and Reevaluation, Meteoritics* **29**, 334–348. https://doi.org/10.1111/j.1945-5100.1994.tb00597.x.

Neal C. R. and Taylor L. A. (1992) Petrogenesis of mare basalts - A record of lunar volcanism. *Geochim. Cosmochim. Acta* **56**, 2177–2211. https://doi.org/10.1016/0016-7037(92)90184-K.

Nemchin A. A., Pidgeon R. T., Whitehouse M. J., Vaughan J. P. and Meyer C. (2008) SIMS U-Pb study of zircon from Apollo 14 and 17 breccias: implications for the evolution of lunar KREEP. *Geochim. Cosmochim. Acta* **72**, 668–689. https://doi.org/10.1016/j.gca.2007.11.009.

Please cite this article in press as: Snape J. F., et al. The timing of basaltic volcanism at the Apollo landing sites. *Geochim. Cosmochim. Acta* (2019), https://doi.org/10.1016/j.gca.2019.07.042

Nemchin A. A., Pidgeon R. T., Healy D., Grange M. L., Whitehouse M. J. and Vaughan J. (2009) The comparative behavior of apatite-zircon U-Pb systems in Apollo 14 breccias: implications for the thermal history of the Fra Mauro Formation. *Meteorit. Planet. Sci.* **44**, 1717–1734. https://doi.org/10.1111/j.1945-5100.2009.tb01202.x.

Nemchin A. A., Whitehouse M. J., Grange M. L. and Muhling J. R. (2011) On the elusive isotopic composition of lunar Pb. *Geochim. Cosmochim. Acta* **75**, 2940–2964. https://doi.org/10.1016/j.gca.2011.02.042.

Nemchin A. A., Grange M. L., Pidgeon R. T. and Meyer C. (2012) Lunar zirconology. *Austral. J. Earth Sci.* **59**, 277–290. https://doi.org/10.1080/08120099.2011.613484.

Nord G. L., Lally J. S., Heuer A. H., Christie J. M., Radcliffe S. V., Griggs D. T. and Fisher R. M. (1973) Petrologic study of igneous and metaigneous rocks from Apollo 15 and 16 using high voltage transmission electron microscopy. Lunar Planet. Sci. IV. Lunar Planet. Inst., Houston. pp. 953–970.

Nunes P. D., Tatsumoto M. and Unruh D. M. (1974) U-Th-Pb systematics of some Apollo 17 lunar samples and implications for a lunar basin excavation chronology. Lunar Planet. Sci. V. Lunar Planet. Inst., Houston. pp. 1487–1514.

Nyquist L. E., Bansal B. M. and Wiesmann H. (1975) Rb-Sr ages and initial 87Sr/86Sr for Apollo 17 basalts and KREEP basalt 15386. Lunar Planet. Sci. VI. Lunar Planet. Inst., Houston. pp. 1445–1465.

Nyquist L. E., Bansal B. M., Wooden J. L. and Wiesmann H. (1977) Sr-isotopic constraints on the petrogenesis of Apollo 12 mare basalts. Lunar Planet. Sci. VIII. Lunar Planet. Inst., Houston. pp. 1383–1415.

Nyquist L. E., Shih C.-Y., Wooden J. L., Bansal B. M. and Wiesmann H. (1979) The Sr and Nd isotopic record of Apollo 12 basalts - Implications for lunar geochemical evolution. Lunar Planet. Sci. X. Lunar Planet. Inst., Houston. pp. 77–114.

Nyquist L. E., Wooden J. L., Shih C.-Y., Wiesmann H. and Bansal B. M. (1981) Isotopic and REE studies of lunar basalt 12038: implications for petrogenesis of aluminous mare basalts. *Earth Planet. Sci. Lett.* **55**, 335–355. https://doi.org/10.1016/0012-821X(81)90162-X.

Nyquist L. E., Lindstrom M., Bansal B. M., Mittlefehldt D., Shih C.-Y. and Wiesmann H. (1989) Chemical and isotopic constraints on the petrogenesis of the large mare basalt clast in breccia 15459. Lunar Planet. Sci. XIX. Lunar Planet. Inst., Houston. pp. 163–174.

Nyquist L. E. and Shih C.-Y. (1992) The isotopic record of lunar volcanism. *Geochim. Cosmochim. Acta* **56**, 2213–2234. https://doi.org/10.1016/0016-7037(92)90185-L.

Paces J. B., Neal C. R., Taylor L. A., Nakai S. and Halliday A. N. (1991) A strontium and neodymium isotopic study of Apollo 17 high-Ti mare basalts - Resolution of ages, evolution of magmas, and origins of source heterogeneities. *Geochim. Cosmochim. Acta* **55**, 2025–12024. https://doi.org/10.1016/0016-7037(91)90040-C.

Papanastassiou D. A. and Wasserburg G. J. (1970) Rb-Sr ages from the ocean of storms. *Earth Planet. Sci. Lett.* **8**, 269–278. https://doi.org/10.1016/0012-821X(70)90111-1.

Papanastassiou D. A. and Wasserburg G. J. (1971a) Rb-Sr ages of igneous rocks from the Apollo 14 mission and the age of the Fra Mauro formation. *Earth Planet. Sci. Lett.* **12**, 36–48. https://doi.org/10.1016/0012-821X(71)90052-5.

Papanastassiou D. A. and Wasserburg G. J. (1971b) Lunar chronology and evolution from Rb-Sr studies of Apollo 11 and 12 samples. *Earth Planet. Sci. Lett.* **11**, 37–62. https://doi.org/10.1016/0012-821X(71)90139-7.

Papanastassiou D. A. and Wasserburg G. J. (1973) Rb-Sr ages and initial strontium in basalts from Apollo 15. *Earth Planet. Sci. Lett.* **17**, 324–337. https://doi.org/10.1016/0012-821X(73)90197-0.

Papanastassiou D. A., Wasserburg G. J. and Burnett D. S. (1970) Rb-Sr ages of lunar rocks from the Sea of Tranquillity. *Earth Planet. Sci. Lett.* **8**, 1–19. https://doi.org/10.1016/0012-821X(70)90093-2.

Papike J. J., Hodges F. N., Bence A. E., Cameron M. and Rhodes J. M. (1976) Mare basalts - Crystal chemistry, mineralogy, and petrology. *Rev. Geophys. Space Phys.* **14**, 475–540. https://doi.org/10.1029/RG014i004p00475.

Premo W. R., Tatsumoto M., Misawa K., Nakamura N. and Kita N. L. (1999) Pb-Isotopic systematics of lunar highland rocks (>3.9 Ga): constraints on early lunar evolution. *Int. Geol. Rev.* **41**, 95–128. https://doi.org/10.1080/00206819909465134.

Prowatke S. and Klemme S. (2006) Trace element partitioning between apatite and silicate melts. *Geochim. Cosmochim. Acta* **70**, 4513–4527. https://doi.org/10.1016/j.gca.2006.06.162.

Qian Y. Q., Xiao L., Zhao S. Y., Zhao J. N., Huang J., Flahaut J., Martinot M., Head J. W., Hiesinger H. and Wang G. X. (2018) Geology and scientific significance of the Rümker region in northern oceanus Procellarum: China's Chang'E-5 landing region. *J. Geophys. Res. (Planets)* **123**, 1407–1430. https://doi.org/10.1029/2018JE005595.

Renne P. R., Balco G., Ludwig K. R., Mundil R. and Min K. (2010) Joint determination of ^{40}K decay constants and ^{40}Ar*/^{40}K for the Fish Canyon sanidine standard, and improved accuracy for ^{40}Ar/ ^{39}Ar geochronology. *Geochim. Cosmochim. Acta* **74**, 5349–5367. https://doi.org/10.1016/j.gca.2010.06.017.

Renne P. R., Balco G., Ludwig K. R., Mundil R. and Min K. (2011) Response to the comment by W.H. Schwarz et al., on "Joint determination of ^{40}K decay constants and ^{40}Ar*/^{40}K for the Fish Canyon sanidine standard, and improved accuracy for ^{40}Ar/ ^{39}Ar geochronology. *Geochim. Cosmochim. Acta* **75**, 5097–5100. https://doi.org/10.1016/j.gca.2011.06.021.

Rhodes J. M. and Hubbard N. J. (1973) Chemistry, classification, and petrogenesis of Apollo 15 mare basalts. Lunar Planet. Sci. IX. Lunar Planet. Inst., Houston. pp. 1127–1148.

Rhodes J. M., Wiesmann H., Rodgers K. V., Brannon J. C., Bansal B. M. and Hubbard N. J. (1976) Chemistry, classification, and petrogenesis of Apollo 17 mare basalts. Lunar Planet. Sci. XII. Lunar Planet. Inst., Houston. pp. 1467–1489.

Rhodes J. M., Brannon J. C., Rodgers K. V., Blanchard D. P. and Dungan M. A. (1977) Chemistry of Apollo 12 mare basalts - Magma types and fractionation processes. Lunar Planet. Sci. VIII. Lunar Planet. Inst., Houston. pp. 1305–1338.

Robbins S. J. (2014) New crater calibrations for the lunar crater-age chronology. *Earth Planet. Sci. Lett.* **403**, 188–198. https://doi.org/10.1016/j.epsl.2014.06.038.

Ryder G. (1990) A distinct variant of high-titanium mare basalt from the Van Serg core, Apollo 17 landing site. *Meteoritics* **25**, 249–258.

Ryder G. (1994) Coincidence in time of the Imbrium Basin impact and Apollo 15 KREEP volcanic flows: The case for impact-induced melting. In *Geological Society of America Special Paper 293* (eds. B. O. Dressler, R. A. F. Grieve and V. Sharpton). Geological Society of America, Boulder, Colorado, pp. 11–18.

Schmitt H. H., Lofgren G., Swann G. A. and Simmons G. (1970) The Apollo 11 samples: Introduction. Lunar Planet. Sci. I. Lunar Planet. Inst., Houston. pp. 1–54.

Schnare D. W., Day J. M. D., Norman M. D., Liu Y. and Taylor L. A. (2008) A laser-ablation ICP-MS study of Apollo 15 low-titanium olivine-normative and quartz-normative mare basalts. *Geochim. Cosmochim. Acta* **72**, 2556–2572. https://doi.org/10.1016/j.gca.2008.02.021.

Please cite this article in press as: Snape J. F., et al. The timing of basaltic volcanism at the Apollo landing sites. *Geochim. Cosmochim. Acta* (2019), https://doi.org/10.1016/j.gca.2019.07.042

Shimizu N. and Hart S. R. (1982) Isotope fractionation in secondary ion mass spectrometry. *J. Appl. Phys.* **53**, 1303–1311. https://doi.org/10.1063/1.330636.

Snape J. F., Nemchin A. A., Grange M. L., Bellucci J. J., Thiessen F. and Whitehouse M. J. (2016a) Phosphate ages in Apollo 14 breccias: resolving multiple impact events with high precision U-Pb SIMS analyses. *Geochim. Cosmochim. Acta* **174**, 13–29. https://doi.org/10.1016/j.gca.2015.11.005.

Snape J. F., Nemchin A. A., Bellucci J. J., Whitehouse M. J., Tartèse R., Barnes J. J., Anand M., Crawford I. A. and Joy K. H. (2016b) Lunar basalt chronology, mantle differentiation and implications for determining the age of the Moon. *Earth Planet. Sci. Lett.* **451**, 149–158. https://doi.org/10.1016/j.epsl.2016.07.026.

Snape J. F., Davids D., Nemchin A. A., Whitehouse M. J. and Bellucci J. J. (2018a) Constraining the timing and sources of volcanism at the Apollo 12 landing site using new Pb isotopic compositions and crystallisation ages. *Chem. Geol.* **482**, 101–112. https://doi.org/10.1016/j.chemgeo.2018.02.009.

Snape J. F., Curran N. M., Whitehouse M. J., Nemchin A. A., Joy K. H., Hopkinson T., Anand M., Bellucci J. J. and Kenny G. G. (2018b) Ancient volcanism on the Moon: insights from Pb isotopes in the MIL 13317 and Kalahari 009 lunar meteorites. *Earth Planet. Sci. Lett.* **502**, 84–95. https://doi.org/10.1016/j.epsl.2018.08.035.

Snyder G. A., Lee D. C., Taylor L. A., Halliday A. N. and Jerde E. A. (1994) Evolution of the upper mantle of the Earth's Moon: neodymium and strontium isotopic constraints from high-Ti mare basalts. *Geochim. Cosmochim. Acta* **58**, 4795–4808. https://doi.org/10.1016/0016-7037(94)90209-7.

Snyder G. A., Hall C. M., Halliday A. N., Lee D. C. and Taylor L. A. (1996) Earliest high-Ti volcanism on the Moon: ^{40}Ar-^{39}Ar, Sm-Nd, and Rb-Sr isotopic studies of Group D basalts from the Apollo 11 landing site. *Meteorit. Planet. Sci.* **31**, 328–334. https://doi.org/10.1111/j.1945-5100.1996.tb02069.x.

Snyder G. A., Neal C. R., Taylor L. A. and Halliday A. N. (1997a) Anatexis of lunar cumulate mantle in time and space: clues from trace-element, strontium, and neodymium isotopic chemistry of parental Apollo 12 basalts. *Geochim. Cosmochim. Acta* **61**, 2731–2747. https://doi.org/10.1016/S0016-7037(97)00082-3.

Snyder G. A., Borg L. E., Lee D. C., Taylor L. A., Nyquist L. E. and Halliday A. N. (1997) Nd-Sr-Hf isotopic and geochronologic studies of Apollo 15 basalts. Lunar Planet. Sci. XXVIII. Lunar Planet. Inst., Houston. p.347 (abstr.).

Snyder G. A., Borg L. E., Lee D. C., Taylor L. A., Nyquist L. E. and Halliday A. N. (1998) Volcanism in the Hadley-Apennine Region of the Moon: Geochronology, Nd-Sr Isotopic Systematics, and Depths of Melting. Lunar Planet. Sci. XXIX. Lunar Planet. Inst., Houston. #1141.

Snyder G. A., Borg L. E., Nyquist L. E. and Taylor L. A. (2000) Chronology and isotopic constraints on lunar evolution. In *Origin of the Earth and Moon* (eds. R. M. Canup and K. Righter). University of Arizona Press, Tucson, Arizona, pp. 361–395.

Sprung P., Kleine T. and Scherer E. E. (2013) Isotopic evidence for chondritic Lu/Hf and Sm/Nd of the Moon. *Earth Planet. Sci. Lett.* **380**, 77–87. https://doi.org/10.1016/j.epsl.2013.08.018.

Spudis P. D. (1978) Composition and origin of the Apennine Bench Formation. Lunar Planet. Sci. IX. Lunar Planet. Inst., Houston. pp. 3379–3394.

Stacey J. S. and Kramers J. D. (1975) Approximation of terrestrial lead isotope evolution by a two-stage model. *Earth Planet. Sci. Lett.* **26**, 207–221. https://doi.org/10.1016/0012-821X(75)90088-6.

Stettler A., Eberhardt P., Geiss J., Grögler N. and Maurer P. (1973) 40Ar-39Ar ages and 38Ar-37Ar exposure ages of lunar rocks. Lunar Planet. Sci. IV. Lunar Planet. Inst., Houston. pp. 1865-1888.

Stöffler D. and Ryder G. (2001) Stratigraphy and isotope ages of lunar geologic units: chronological standard for the inner solar system. *Space Sci. Rev.* **96**, 9–54. https://doi.org/10.1023/A:1011937020193.

Tartèse R., Anand M. and Delhaye T. (2013) NanoSIMS Pb/Pb dating of tranquillityite in high-Ti lunar basalts: implications for the chronology of high-Ti volcanism on the Moon. *Am. Mineral.* **98**, 1477–1486. https://doi.org/10.2138/am.2013.4467.

Tatsumoto M. (1970) Age of the moon: An isotopic study of U-Th-Pb systematics of Apollo 11 lunar samples-II. Lunar Planet. Sci. I. Lunar Planet. Inst., Houston. pp. 1595–1612.

Tatsumoto M., Hedge C. E., Doe B. R. and Unruh D. M. (1972a) U-Th-Pb and Rb-Sr measurements on some Apollo 14 lunar samples. Lunar Planet. Sci. IV. Lunar Planet. Inst., Houston. pp. 1531–1555.

Tatsumoto M., Hedge C. E., Knight R. J., Unruh D. M. and Doe B. R. (1972b) U-Th-Pb, Rb-Sr, and K measurements on some Apollo 15 and Apollo 16 samples. The Apollo 15 Lunar Samples. Lunar Planet. Inst., Houston pp. 391–395.

Taylor G. J., Martel L. M. V. and Spudis P. D. (2012) The Hadley-Apennine KREEP basalt igneous province. *Meteorit. Planet. Sci.* **47**, 861–879. https://doi.org/10.1111/j.1945-5100.2012.01364.x.

Taylor L. A., Patchen A., Mayne R. G. and Taylor D.-H. (2004) The most reduced rock from the moon, Apollo 14 basalt 14053: Its unique features and their origin. *Am. Mineral.* **89**, 1617–1624. https://doi.org/10.2138/am-2004-11-1205.

Tera F. and Wasserburg G. J. (1972) U-Th-Pb systematics in three Apollo 14 basalts and the problem of initial Pb in lunar rocks. *Earth Planet. Sci. Lett.* **14**, 281–304. https://doi.org/10.1016/0012-821X(72)90128-8.

Tera F. and Wasserburg G. J. (1974) U-Th-Pb systematics on lunar rocks and inferences about lunar evolution and the age of the Moon. Lunar Planet. Sci. V. Lunar Planet. Inst., Houston. pp. 1571–1599.

Thiessen F., Nemchin A. A., Snape J. F., Whitehouse M. J. and Bellucci J. J. (2017) Impact history of the Apollo 17 landing site revealed by U-Pb SIMS ages. *Meteorit. Planet. Sci.* **52**, 584–611. https://doi.org/10.1111/maps.12814.

Thiessen F., Nemchin A. A., Snape J. F., Bellucci J. J. and Whitehouse M. J. (2018) Apollo 12 breccia 12013: impact-induced partial Pb loss in zircon and its implications for lunar geochronology. *Geochim. Cosmochim. Acta* **230**, 94–111. https://doi.org/10.1016/j.gca.2018.03.023.

Tilton G. R. and Chen J. H. (1979) Lead isotope systematics of three Apollo 17 mare basalts. Lunar Planet. Sci. X. Lunar Planet. Inst., Houston. pp. 259–274.

Turner G. (1970) Argon-40/argon-39 dating of lunar rock samples. Lunar Planet. Sci. I. Lunar Planet. Inst., Houston. pp. 1665–1684.

Turner G. (1971) ^{40}Ar-^{39}Ar ages from the lunar maria. *Earth Planet. Sci. Lett.* **11**, 169–191. https://doi.org/10.1016/0012-821X(71)90161-0.

Turner G., Huneke J. C., Podosek F. A. and Wasserburg G. J. (1971) ^{40}Ar-^{39}Ar ages and cosmic ray exposure ages of Apollo 14 samples. *Earth Planet. Sci. Lett.* **12**, 19–35. https://doi.org/10.1016/0012-821X(71)90051-3.

Turner G., Cadogan P. H. and Yonge C. J. (1973) Argon selenochronology. Lunar Planet. Sci. IV. Lunar Planet. Inst., Houston. pp. 1889–1914.

Unruh D. M. and Tatsumoto M. (1977) Evolution of mare basalts - The complexity of the U-Th-Pb system. Lunar Planet. Sci. VIII. Lunar Planet. Inst., Houston. pp. 1673–1696.

Please cite this article in press as: Snape J. F., et al. The timing of basaltic volcanism at the Apollo landing sites. *Geochim. Cosmochim. Acta* (2019), https://doi.org/10.1016/j.gca.2019.07.042

Villa I. M., De Bièvre P., Holden N. E. and Renne P. R. (2015) IUPAC-IUGS recommendation on the half life of ^{87}Rb. *Geochim. Cosmochim. Acta* **164**, 382–385. https://doi.org/10.1016/j.gca.2015.05.025.

Warner R. D., Taylor G. J., Conrad G. H., Northrop H. R., Barker S., Keil K., Ma M.–S. and Schmitt R. (1979) Apollo 17 high-Ti mare basalts - New bulk compositional data, magma types, and petrogenesis. Lunar Planet. Sci. X. Lunar Planet. Inst., Houston. pp. 225–247.

Whitehouse M. J., Kamber B. S., Fedo C. M. and Lepland A. (2005) Integrated Pb- and S-isotope investigation of sulphide minerals from the early Archaean of southwest Greenland. *Chem. Geol.* **222**, 112–131. https://doi.org/10.1016/j.chemgeo.2005.06.004.

Woodhead J. D. and Hergt J. M. (2000) Pb-Isotope analyses of USGS reference materials. *Geostand. Geoanal. Res.* **24**, 33–38. https://doi.org/10.1111/j.1751-908X.2000.tb00584.x.

York D., Kenyon W. J. and Doyle R. J. (1972) 40Ar-39Ar ages of Apollo 14 and 15 samples. Lunar Planet. Sci. III. Lunar Planet. Inst., Houston. pp. 1613–1622.

Associate editor: James M.D. Day